Electromagnetic Absorbers Based on Frequency Selective Surfaces

Filippo Costa [(1)] Alireza Kazemzadeh [(2)] Simone Genovesi [(1)] Agostino Monorchio [(1)]

[(1)] University of Pisa

Email: filippo.costa(simone.genovesi,a.monorchio)@iet.unipi.it

[(2)] GKN Aerospace

Email: Alireza.Kazemzadeh@gknaerospace.com

Abstract— Frequency Selective Surfaces (FSSs) are bidimensional arrays of particles arranged in a periodic manner. These surfaces can be lossless or lossy depending on the manufacturing process. They can be fabricated by using metallic or controlled-resistance surface deposition. Lossy surfaces can be also obtained through the integration of lumped components on a metallic surface. The use of FSSs has fostered new research lines in the design of electromagnetic absorbing surfaces bringing improvements both in terms of bandwidth/thickness ratio maximization and in terms of customizability of the absorbing bandwidth (narrowband, multi-band, wideband, ultra-wideband) for specific applications. Artificial impedance surfaces (or High-Impedance Surfaces, - HIS) are thin resonant cavities synthesized by printing a periodic frequency selective surface on the top of a grounded dielectric slab. By a proper tailoring of the geometrical and electrical properties of the FSS, as well as the substrate, several electrically-thin absorbing designs can be obtained. Ultra-narrowband absorbers with extremely stable angular behavior, often addressed as metamaterial absorbers, can be realized by exploiting only dielectric losses of commercial substrates. Narrowband, wideband and ultra-wideband configurations are instead implemented by also resorting to ohmic losses in a non-conducive FSS. A thorough review of the available absorbers will be presented together with multi-band and tunable design techniques. Manufacturing processes and practical examples will be also addressed and the most interesting fields of application of the presented structures will be described.

Index Terms — Artificial Magnetic Conductor (AMC), Artificial Impedance Surface (AIS), Electromagnetic Absorbers, Frequency Selective Surface (FSS), High Impedance Surfaces (HIS), Metamaterial.

I. INTRODUCTION

Recent developments in the synthesis of metamaterials have generated a great interest on thin electromagnetic absorbing structures due to the high number of practical applications spanning from microwaves to optical frequencies. At microwave frequencies thin absorbing structures are beneficial to reduce the radar signature of targets [1]–[5], to improve the electromagnetic compatibility of devices [6], to avoid multiple reflections in complex indoor environments, to minimize mutual coupling between antennas or to synthesize power imaging devices [7]. A wide operating bandwidth is one of the main requirements across the microwave range while frequency selective ultra-narrowband absorbing structures are more desirable in THz range to design novel devices such as photodetectors, microbolometers [8], [9] or phase modulators [10]. Promising applications of metamaterial absorbers at optical frequencies regard the use of such structures as frequency selective emitters to improve the efficiency of conventional and thermophotovoltaic solar cells [11], [12].

The possibility of employing frequency selective surfaces for reducing the thickness of the classical absorbing structures (Salisbury, Jaumann and Dallenbach screens [13]) has been intensively investigated , particularly in the last decade, even if there exist older publications on periodic surfaces employed in absorbers design [14]–[16]. FSS-based absorbers can be partitioned into two main categories: those employing lossy FSSs and those employing metalized FSSs. The former class employs lossy FSS in order to minimize scattered energy through ohmic and dielectric dissipation in a reduced thickness. Lossy FSSs usually replace uniform lossy layers, such as in Salisbury or Jaumann absorbers, in order to introduce a reactive part into surface impedance together with a resistive component. Lossy surfaces can be synthesized either by employing a resistors in each unit cell of the periodic surface on a metallic surface [17]–[19] or by printing periodic shapes using resistive inks [20]. On the other hand, metallic FSSs can be employed in conjunctions with uniform lossy sheets in order to provide larger or multi-band operating bands [21]–[23]. More recently fully metallic FSS-based absorbers were proposed to achieve perfect absorption (single frequency, absorption at all incident angles) through the maximizations of the dielectric dissipation [24], [25].

A simple layout allowing the synthesis of both ultra-narrowband, narrowband, wideband and ultra-wideband electrically-thin absorbers is the High-Impedance Surface (HIS) formed by a thin substrate, a frequency selective surface with a suitable shaped element and a ground plane.
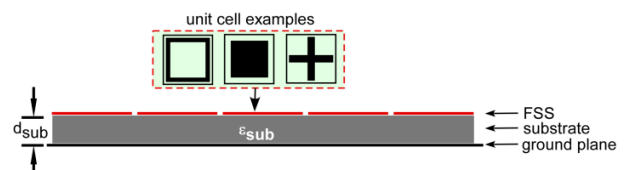

Fig. 1 – Side view of an Artificial Impedance Surface (AIS) absorber.

This configuration is also known as Artificial Impedance Surface (AIS) because of its ability to act as an impedance boundary condition. Generally, the electric and geometric characteristics of the dielectric substrate are imposed as initial design parameters or can be chosen among an available set of materials. For this reason, a correct choice of the frequency selective surface elements is of vital importance for designing the absorber with the desired characteristics. The suitable amount of loss can be introduced in the resonant FSS structure (or near to it) or in the dielectric substrate or in both of them. The absorbing structure can be optimized through a genetic algorithm [26], [27] or by using a simple equivalent circuit model. The latter approach is preferred in this article since it allows to get physical insight into absorbing mechanisms.

Ultra-narrowband absorption is obtained by exploiting dielectric losses of the commercial substrates only. This kind of structures are frequently referred to as Perfect Metamaterial Absorbers [24] and are mostly investigated by physicists across THz gap and within the visible part of the electromagnetic spectrum even if they were also proposed for Sub-GHz communication applications with very low-cost manufacturing process [25]. As the ohmic losses are introduced close to the periodic pattern by use of resistive sheets [28] or directly in the periodic pattern through lumped resistors [17], [29] or resistive inks [20], the absorption bandwidth can be greatly enlarged. The bandwidth can be either narrow or wide depending on the number of parallel resonances (inductive-capacitive impedances connected in parallel) involved in the design. Two resonances can be introduced both by designing a single resonant [30] or multi-resonant FSS elements [31] and by stacking more FSS layers [32]–[34]. The absorber can be efficiently analyzed by an equivalent transmission-line (TL) model [35].

II. Classification of absorbing structures

The artificial impedance surface displayed in Fig. 1 acts as a resonant cavity. The amount of power absorbed by the resonant cavity at the resonance is determined by the value of the real part of the input impedance since the imaginary part of the input impedance of a lossy structure is close to zero at the resonance. The magnitude of the reflection coefficient at the resonance of the cavity approximately reads [36]:

$$|\Gamma| \approx \frac{\text{Re}\{Z_{HIS}\} - \zeta_0}{\text{Re}\{Z_{HIS}\} + \zeta_0} \qquad (1)$$

where Z_{HIS} represents the input impedance of the absorbing HIS structure and ζ_0 is the characteristic impedance of free space at normal incidence. The input impedance of the HIS structure is equal to the parallel connection between the two complex impedances Z_{FSS} and Z_d which represent the FSS impedance and grounded substrate impedance, respectively. The impedances of the grounded substrate and the frequency selective surface in presence of a lossless or even lossy dielectric can be computed analytically on the basis of some well justified approximations. By deriving an explicit expression of the real part of the input impedance of the impedance surface, which is directly related to the amount of

loss at the resonance, several properties of the AIS absorber having immediate practical implications can be easily extracted. A series LC circuit can model the impedance of a frequency selective surface and a couple of resistors can take into account both dielectric and ohmic losses:

$$Z_{FSS} = R_0 + R_D + \left(1 - \omega^2 LC\right) / \left(j\omega C\right) \qquad (2)$$

where C and L represent the capacitance and the inductance of the FSS. The spacing between the edges of the elements controls the capacitance, and the magnetic flux created between the patches and the ground plane defines the inductance. The capacitance of an FSS printed on a dielectric substrate is computed by multiplying the unloaded capacitor by the real part of the effective dielectric permittivity due the surrounding dielectrics. The capacitor formed between the adjacent elements has a loss component since the electric field lines are concentrated in a lossy medium. Such loss component is readily represented by the following series resistor [36]:

$$R_D \approx \frac{\varepsilon_r^{''}}{\omega C \left(\varepsilon_r^{'} + 1\right)} \qquad (3)$$

The FSS series resistor R_D is inversely proportional to the FSS capacitance. The ohmic resistor connected in series with the aforementioned dielectric resistor can be evaluated by weighting the classical expression of the surface resistance valid for metals or resistive inks with the ratio between metalized area and periodicity of the unit cell:

$$\begin{aligned} R_o &\approx \frac{S}{A} \frac{1}{\sigma \delta} \quad if \ \ t < \delta \\ R_o &\approx \frac{S}{A} \frac{1}{\sigma t} \quad if \ \ t > \delta \end{aligned} \qquad (4)$$

where t, δ and σ represent the thickness, the skin-depth and the electrical conductivity of the metallic/resistive pattern, respectively. S is equal to D^2, D is the cell periodicity and A is the surface area of the lossy element within a single unit cell. The relation (4) implies that an element with small scattering area (*e.g.* cross), require a higher surface resistance than an element with a large scattering area (*e.g.* patch) [20].
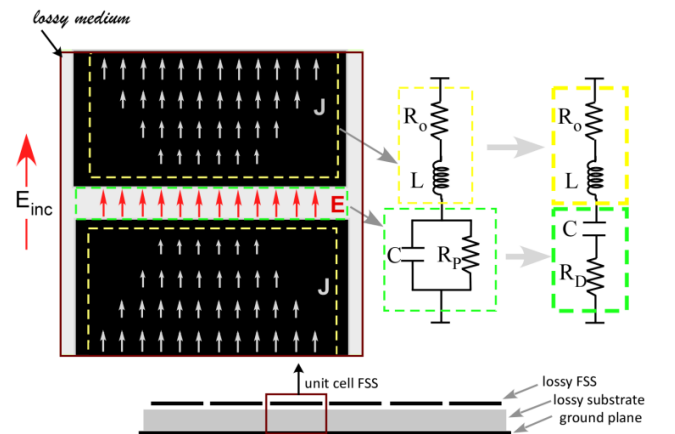

Fig. 2 – Pictorial representation of the physical significance of the proposed equivalent circuit.

If the FSS is made of copper, ohmic losses obtained according to relation (4) are generally two orders of magnitude lower than the dielectric resistor (3). Conversely, if the metal is replaced with a resistive ink, the resistor is larger than the dielectric resistor. Ohmic losses comes from the currents flowing on an imperfect conductor and they are increasingly important as the working frequency raises. As matter of fact, the ohmic resistor is comparable with the dielectric one in THz range and it dominates across optical regime [37]. A pictorial representation of the equivalent circuit of the FSS embedded in a lossy medium is reported in Fig. 2.

At the resonance of the lossy structure, the imaginary part of the input impedance Z_H crosses the zero. After some simple algebraic operations, the real part of the input impedance Z_H at the resonance is derived [20], [36]:

$$\text{Re}\left\{Z_H^{res}\right\} \simeq \frac{\left(\text{Im}\{Z_d\}\right)^2}{\left(\text{Re}\{Z_d\} + R_O + R_D\right)} \qquad (5)$$

The expression in (5) contains all the degrees of freedom of the HIS absorber: it is a function of the FSS capacitance, of the electrical substrate thickness and of the real and imaginary part of the dielectric permittivity. Since $\text{Re}\{Z_d\}$ is usually much smaller than $\text{Re}\{Z_{FSS}\}$ at the main resonance of the HIS [36], relation (5)can be explicated as:

$$\text{Re}\left\{Z_H^{res}\right\} = \frac{\dfrac{\zeta_0^2}{\varepsilon_r'}\left[tg^2\left(k_0 d\sqrt{\varepsilon_r'}\right)\right]}{\left(\dfrac{D}{L}\right)^2 \dfrac{1}{\delta\sigma} + \dfrac{-2\varepsilon_r''}{\omega_0 C_0\left(\varepsilon_r'+1\right)^2}} \qquad (6)$$

where ω_0 is the first resonance frequency.

Depending of the prevalent nature of losses, different type of absorbers can be identified from relations (5) and (6) [38]:

- $R_D \gg R_O$: Ohmic losses negligible with respect to dielectric losses. The loss component is determined by the substrate properties. The substrate thickness and the FSS element needs to be chosen in order to maximize the absorption at the desired frequency. The structure is typically *ultra-narrowband*.

- $R_D \sim R_O$: Both ohmic and dielectric losses contribute to absorption at the resonance. The resistors' values are typically comparable in THz range because ohmic losses start to play an important role also for metallic structures. R_D and R_O can assume comparable values also in the microwave range if low-loss substrates are employed. The structure is typically *ultra-narrowband* or *narrowband*.

- $R_O \gg R_D$: Ohmic losses are predominant. It is typically the case of lossy frequency selective surfaces manufactured with resistive inks or loaded with lumped resistors. Ohmic losses are predominant also in optical range even if the structure is completely metallic. The structure is typically *narrowband, wideband or ultra-wideband*.

III. ULTRA-NARROWBAND AND NARROWBAND CONFIGURATION

The difference between HIS absorbers made up of metallic or resistive FSSs are clarified through a numerical example. In Fig. 3a the dielectric and the ohmic resistance of the FSS impedance are compared with the real part of the substrate input impedance for a HIS absorber comprising a simple cross shaped FSS. The substrate is a commercial FR4. The curves obtained through the approximate relations are compared with those obtained by using Method of Moments simulations [39]. In the case of metallic FSS the dielectric resistor is much higher than the ohmic resistor while in the case of resistive FSS losses introduced in the periodic pattern make the ohmic resistor predominant. The use of metallic FSSs forces the choice of the substrate thickness for obtaining, according to relation (6), a value of the real part of the HIS input impedance close to the free space impedance at the resonance.
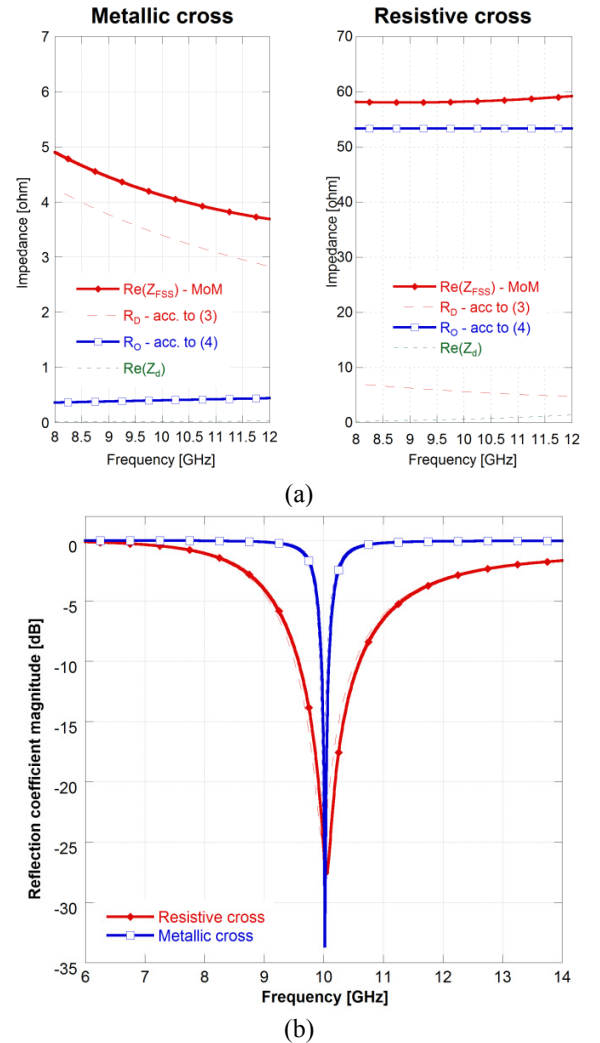

(a)

(b)

Fig. 3 - (a) Dielectric and ohmic components of the real part of the FSS impedance compared with the real part of the grounded substrate input impedance for absorbing structures comprising a metallic or a resistive FSS. (b) Reflection coefficient of the HIS absorber comprising both metallic and resistive FSSs. Continuous line: MoM simulation, Dashed line: Transmission line model.

The FSS element is the same in both cases but the periodicity of the metallic cross is slightly higher than the periodicity of the resistive cross in order to have absorption at the same frequency. The substrate thickness chosen for perfect absorption in the case of metallic cross is 0.5 mm while the substrate thickness for the resistive cross case is 1.6 mm. The lower substrate thickness increases FSS capacitance due to the influence of high-order Floquet modes. In the Fig. 3b the reflection coefficient of the thin absorber comprising a metallic and a resistive cross is shown. Due to the very small substrate thickness, the absorption bandwidth of the metallic absorber is ultra-narrow. The use of resistive patterns introduces an additional degree of freedom in (6). For this reason, the substrate thickness leading to a matching of the HIS input impedance with the free space impedance can be arbitrary selected. In order to maintain a perfect absorption at the resonance while the substrate thickness is increased, the surface resistance of the FSS needs to be enhanced (narrowband case). The bandwidth of the absorber is directly proportional on the substrate thickness but, once the substrate thickness is fixed, the use of tightly coupled patch arrays allows to maximize the absorption bandwidth [40]. It is worth to point out the use of exotic elements is not necessary for obtaining a narrowband absorption. An optimal tuning can be simply obtained by Jerusalem cross element. More complex FSS elements are instead very useful for achieving wideband performance.

IV. BANDWIDTH OF NARROWBAND ABSORBERS

The bandwidth of the above-described narrowband absorbing configurations depends both on substrate properties and on FSS unit cell. Large substrate thickness leads to bandwidth enhancement but increased thickness is undesired in absorber design. For practical purposes it is useful to understand how to select FSS shapes in order to maximize or minimize absorption bandwidth, while the substrate geometrical and electrical properties are kept unchanged.
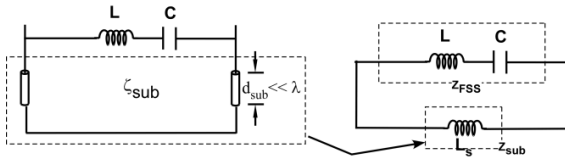

Fig. 4 - Equivalent transmission line of a high-impedance surface and its corresponding lumped circuit model allowing to correctly determine the bandwidth of the structure.

By using the equivalent circuit of Fig. 4, valid for lossless AISs, it is possible to derive physical bandwidth limits and to obtain guidelines for tailoring the operating bandwidth of the absorber. The impedance of the circuit reads:

$$Z = j \frac{\omega L_s \left(1 - \omega^2 LC\right)}{1 - \omega^2 C \left(L + L_s\right)} \quad . \quad (7)$$

The bandwidth of a high-impedance surface is defined as the frequency range where the absolute value of the impedance is larger than the free space impedance, that is, phase of reflection coefficient between [+90,-90°]. By solving equation for $+\zeta_0$ and $-\zeta_0$ with the theory of the cubic equations, the fractional bandwidth, $FBW = \left(\omega_{-\zeta_0} - \omega_{+\zeta_0}\right)\big/\omega_0$, of the circuit is obtained [40]:

$$FBW = \sqrt{C\left(L + L_S\right)} \left[\sqrt{-Q}\left(\cos\left(\vartheta\right) + \sqrt{3}\sin\left(\vartheta\right)\right) - \frac{2}{3}A_2\right] \quad (8)$$

where $A_2 = -\sqrt{\zeta_0\left(L_s + L\right)}\big/L_s L$, $A_1 = -1/LC$, $A_0 = \pm\zeta_0/L_s LC$

$Q = \left(3A_1 - A_2^2\right)\big/9$, $R = \left(9A_1 A_2 - 27A_0 - 2A_2^3\right)\big/54$ and

$\vartheta = \cos^{-1}\left(R\big/\sqrt{-Q^3}\right)$. In order to highlight how the FSS series inductance and the substrate inductance influence fractional bandwidth of high-impedance surfaces, the relation (8) is shown in Fig. 5 as a function of L_S and L. When the value of the inductance is varied, the capacitance value is changed as well, in order to maintain the resonance frequency fixed.
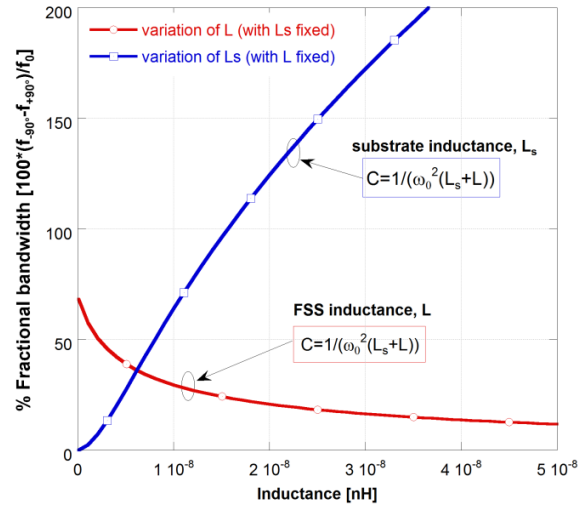

Fig. 5 - Fractional bandwidth of a high-impedance surface as a function of the FSS series inductance L (by fixing the grounded substrate inductance Ls to 7 nH) and as a function of Ls (by fixing L to 4 nH) . The capacitance is varied in order to preserve the same resonance frequency that is fixed to 6 GHz in all cases. Figure reproduced with permission [40]. Copyright 2013, IEEE.

As expected, increasing the grounded substrate inductance leads to a robust enlargement of the fractional bandwidth. Once that substrate thickness (inductance) is fixed, the fractional bandwidth of the resonant circuit can be maximized by decreasing the FSS *series* inductance. The capacitance increase is changed time to time in order to keep the resonant frequency, that is electrical thickness of the substrate, unchanged. Theoretical limitation is represented by the condition $L=0$. This condition is approached when a patch array with a very small gap is employed. On the other hand, absorbers with high quality factor can be designed by using elements with high inductance (for example thin crosses).

To prove these arguments some representative FSS shapes are simulated on the same grounded dielectric substrate. The substrate parameters are $\varepsilon_r = 4.5 - j0.088$ and thickness equal to

1.6 mm. Patch elements characterized by a different ratio R between the patch size L and the periodicity D ($R=L/D$) are analyzed since they are characterized by a different value of inductance and capacitance still preserving the same negative impedance value at the resonance of the HIS. The patch with smallest gap has the highest capacitance and the smallest inductance. The cross-shaped FSS is characterized by a high inductance and a small capacitance. For the meandered shape the capacitance gives a stronger contribution than inductance even if they are both very high. Indeed, to achieve the resonance of the meandered shaped AIS at the same frequency of the other elements a high degree of miniaturization is applied to the periodicity. Fig. 5 shows the phase of reflection coefficient of different HIS. The L and C of the unit cells are determined to verify the model [40]. As expected, the bandwidth of the cross element is the smallest whereas, among the patches, a higher ratio R leads to a larger bandwidth of the FSS. The meandered structure is characterized both by a high capacitance, due to the strong coupling between adjacent lines, and a high inductance due to the narrowness and the length of the lines. Indeed, these high values are instrumental for a substantial miniaturization of the unit cell.
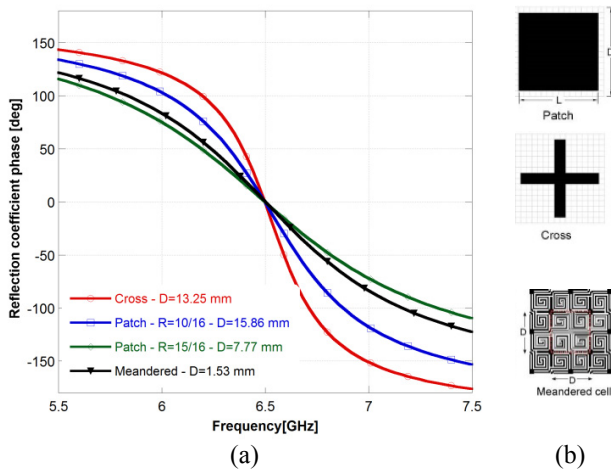

(a)   (b)

Fig. 6 - Phase of reflection coefficient of different HIS (a) on the same substrate and a periodicity (D) designed so that all the analyzed structures resonate at the same frequency. (b) geometry of the analyzed unit cells. Figure reproduced with permission [40]. Copyright 2009, IEEE.

V. BANDWIDTH ENLARGEMENT TECHNIQUES

Techniques to improve the matching bandwidth of subwavelength absorbers are based either on substrate properties modification or on the use of more complicated FSS element geometry.

a) bandwidth enlargement by using magnetic substrates

The use of a magnetic substrate instead of an electric one is a simple strategy to improve the absorption bandwidth [41]–[43]. The effectiveness of this strategy can be demonstrated by simply inspecting the analytic expression of the grounded substrate inductance used in the previous section:

$$Z_d = j\omega L_s = j\zeta_0 \sqrt{\frac{\mu_r}{\varepsilon_r}} \tan\left(2\pi \frac{d}{\lambda_0} \sqrt{\varepsilon_r \mu_r}\right) \quad (9)$$

Keeping constant the quantity inside the brackets, so that the electrical thickness is not changed, it is evident that the use of a high magnetic permeability brings an increase of the substrate inductance while the use of a high dielectric permittivity produces the opposite trend. From Fig. 5, it is apparent that the use of a high substrate inductance is a very good strategy for improving the bandwidth even if the resonance frequency is kept constant by changing the FSS capacitance. Clearly, the drawback of this solution is the weight of the absorber, which dramatically increases. A comparison of achievable bandwidth performance for an ultra-thin resonant absorber comprising air, dielectric or magnetic substrates is shown in Fig. 7. The electrical thickness of the absorber is kept constant for the three analyzed configurations ($\lambda_g/30$) and the parameters of the patch type FSS are chosen in order to get the resonance at the same frequency.
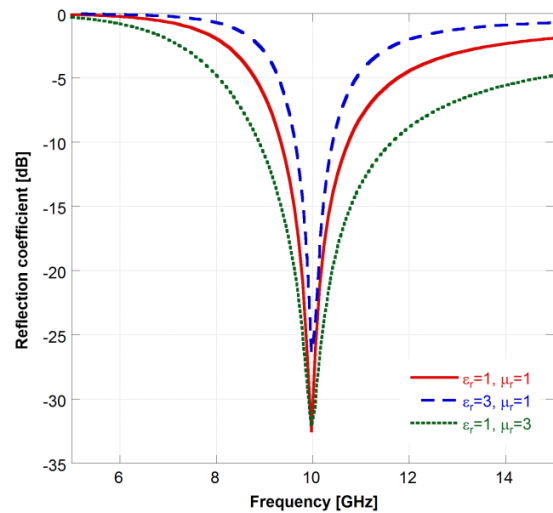

Fig. 7 – Absorption performance with air substrate, dielectric substrate and magnetic substrate. The electrical thickness of the absorber is kept constant for the three analyzed configurations: it is equal to 1mm ($\lambda g/30$) in the air substrate case and 0.577 mm for the other two configurations. The FSS parameters are set in order to achieve the resonance at the same frequency.

b) bandwidth enlargement by using multi-resonant dipoles on the same unit cell

One possibility to improve the absorption bandwidth is to use multiple resonances located close to each other. Multiples dipole elements can be used for enlarging absorption band. One method utilizes multiple resonating structures in each unit cell, exploiting the fact that resonators with different sizes resonate at different frequencies. If the resonance frequencies of the resonators are close enough the absorption band of the ultra-thin metamaterial absorber, the absorption band can be potentially enlarged. However, it has to be pointed out that this methodology works only if the surface resistance of each resonator in the unit cell is adequately controlled. The surface resistance of large elements must be higher than the surface resistance of small

elements. As an example, the reflection coefficient of a tri-dipole unit cell arranged on both the incident planes is reported in Fig. 8. The length and the optimal surface resistances of the three dipole are 5.1 mm, 3.9 mm, 3.3 mm and 4 $\Omega\square^{-1}$, 4.5 $\Omega\square^{-1}$, 0.05 $\Omega\square^{-1}$, respectively. The dependence of the reflection coefficient on the surface resistance value of the smallest dipole element is highlighted in figure.
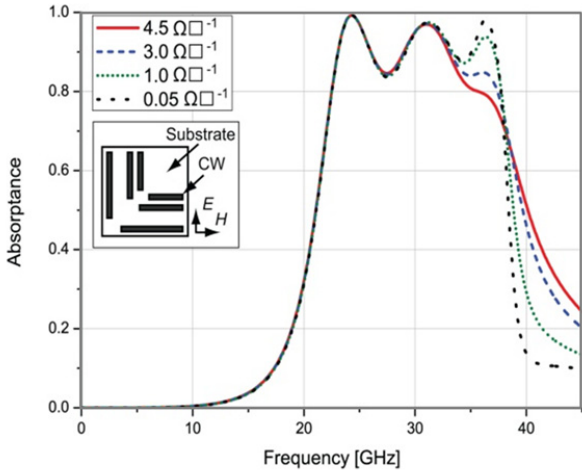

Fig. 8 - Absorption of three dipoles (5.1, 3.9 and 3.3 mm). Modification of the resistance value used for the 3.3 mm dipoles leads to the triple absorption peak. Figure reproduced with permission [44]. Copyright 2012, Optical American Society.

c) bandwidth enlargement by using single-resonant resonators located on separate layers

Another technique proposed to enlarge the bandwidth of metamaterial absorbers is stacking the same resonator with different geometrical characteristics on multiple layers. In this way the coupling between closely spaced elements is reduced with respect to configurations where multi-resonant elements are located on the same layers. This disposition leads to a more complex multilayer structure which still preserves a considerable subwavelength profile. For instance in [45] a multi-loop absorber is proposed.
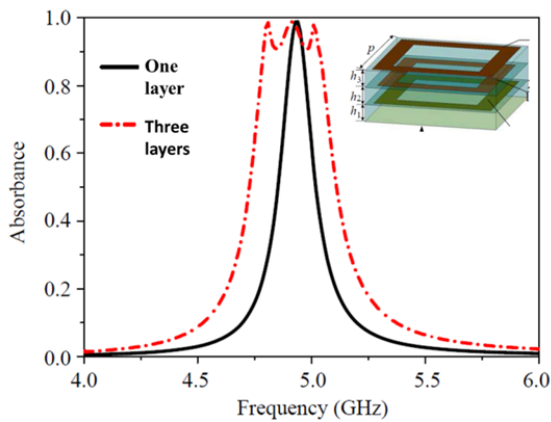

Fig. 9 - Simulated absorbing performance for of the multi-loop absorber at normal incidence compared with the absorption behavior obtained with a single resonant and single layer absorber. Figure reproduced with permission. Courtesy of The Electromagnetics Academy [45].

The loop resonators are printed on the top of FR4 dielectric slabs with thickness of 0.3mm. The electric size of this absorber is roughly $\lambda_g/32$. The reflection coefficient of the multi-loop absorber is shown in Fig. 9.

VI. MULTI-RESONANT FSS ABSORBERS

When metallic concentric loop elements are employed on the same periodic surface a multi-resonant absorption behavior can be achieved. As depicted in Fig. 10, an FSS unit cell with several concentric loops leads to close resonances in the reflection profile. As depicted in Fig. 10, a multi-loop FSS can be represented as a shunt connection of several series RLC circuits. The number of absorption peaks is related to the number of loops. As an example, the reflection coefficient of a five-loop unit cell is reported in Fig. 11. Both the normal and oblique incidence response are reported to remark that the position of the resonance frequencies is nearly unaffected by the angle variation leading to a very stable absorption properties. From a circuit point of view, angular stability of the absorption is achieved since the impedance of the thin grounded substrate is nearly unaffected by the variation of the incident angle and also the FSS impedance of thin loop elements is angularly stable [46]. It has to be noticed that the matching condition (perfect absorption) is different for the first resonance with respect to high order ones. It can happen that the real part of the input impedance associated with the first loop is larger than free space impedance and, at the same time, the real part of the input impedance associated with high order resonance is lower than free space impedance. In this situation, a decrease of the substrate thickness leads to an improved matching with free space for the first resonance but a suboptimal matching for higher order resonances. In relation to this, it is important to select a substrate with a suitable thickness and the proper amount of substrate losses to guarantee good absorption at all resonant frequencies.
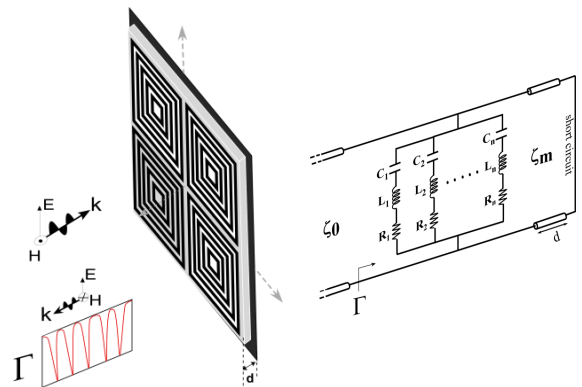

Fig. 10 - (a) 3D sketch of the multi-band absorber comprising 2×2 unit cells, (b) Equivalent circuit model. Each Ri Li Ci series is related to the particular i-th loop of the unit cell. Figure reproduced with permission [47]. Copyright 2013, IEEE.

In practice, the structure can be truncated to a few unit cells (2×2 or 3×3) preserving the absorption properties obtained with the periodic simulation. The number of unit cells employed impacts on the value of backscattered field therefore the number of unit cells can be chosen to obtain the

desired radar cross section. The multi-loop absorber can be efficiently used as a chipless RFID tag [47]. Being each resonance determined by a specific concentric loop, the presence or the absence of a loop is used to apply an amplitude modulation on the reflected signal.
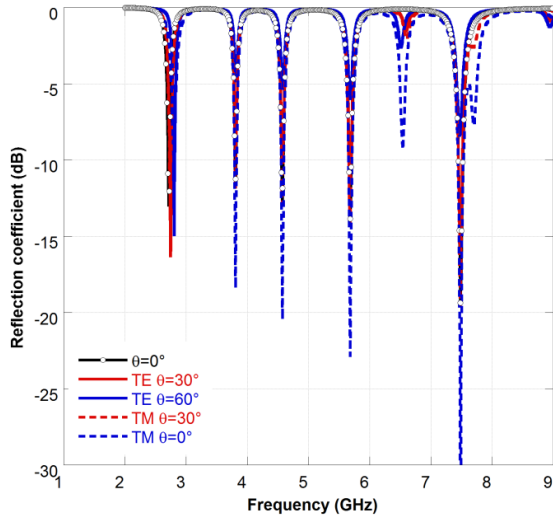

Fig. 11 - Reflection coefficient of an infinite HIS comprising a double square loop unit cell on top of a 1.6 mm FR4 substrate. TE and TM behavior at normal and oblique incidence are reported. Figure reproduced with permission [47]. Copyright 2013, IEEE.

VII. Oblique incidence performance improvement by using electric or magnetic plasmonic resonances in the substrate

As it is well known, a wire medium behaves as a plasma around at a certain resonance frequency dictated by the radius and the periodicity of the wires [48]–[50]. Moreover, when vias are loaded with metallic patches the spatial dispersion is suppressed [51] leading to a plasmonic resonance nearly independent on incident angle. Presence of vias can be therefore advantageously used to enlarge the absorption bandwidth at oblique incidence [52]. The proposed methodology consists in designing the wire medium formed by the array of vias so that the plasma resonance occurs in the vicinity of the HIS resonance. When the incident angle of the TM polarized waves is off from the normal direction, part of the electric field is aligned to shorting vias and an additional resonance is created in the absorption profile. As the incidence angle grows the plasma resonance becomes stronger and absorption is increased. The position of the resonance is determined by the radius of the vias and therefore can be shifted independently of the main AMC resonance. Its position can be efficiently estimated through a rigorous analytical approach [52], [53]. The typical behavior of the phase of the TM reflection coefficient of a AIS both for normal and oblique incidence is shown in Fig. 12. The figure highlights the effect of vias radius: plasma resonance shifts towards lower frequencies as the vias radius is reduced.

As an example of the performance of the absorbing layer, an artificial impedance surface with the following parameters

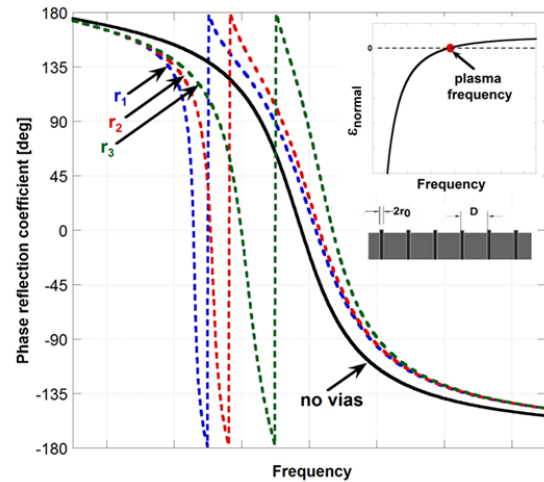is considered: $D = 10$ mm, $L = 8.75$ mm, $d = 3$ mm, $\varepsilon_r = 2(1 - j0.5)$ and $r_0 = 0.1$ mm.

Fig. 12 - Typical reflection coefficient at oblique incidence for TM polarization without vias and in presence of vias with different radius (r1<r2<r3). Inset: Typical behavior of the normal relative dielectric permittivity in the uniaxial grounded wire array.

In this example, losses are in the dielectric slab but the methodology can be applied in the case of resistive frequency selective surfaces. We see notable enlargement of the absorption band when the vias are included into the design. Vias have no effect on TE polarization.
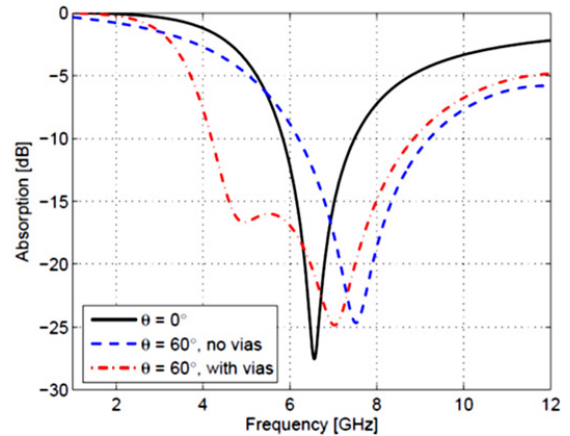

Fig. 13 - TM reflection coefficient at 60° with and without vias.

However, a similar effect can be obtained for TE polarization by introducing a magnetic plasmonic resonance in the substrate [54]. This can be done for instance by loading the substrate with split ring resonators coupled with magnetic fields. In [54] a capacitive array of square resistive patches is placed on top of a 2.0 mm thick meta-backed substrate. The reflection coefficient of the periodic surface is reported in Fig. 14. When the magnetic field is perpendicular to the SRR, two absorption peaks are clearly present at the frequencies of 5.9 GHz and 6.7 GHz.
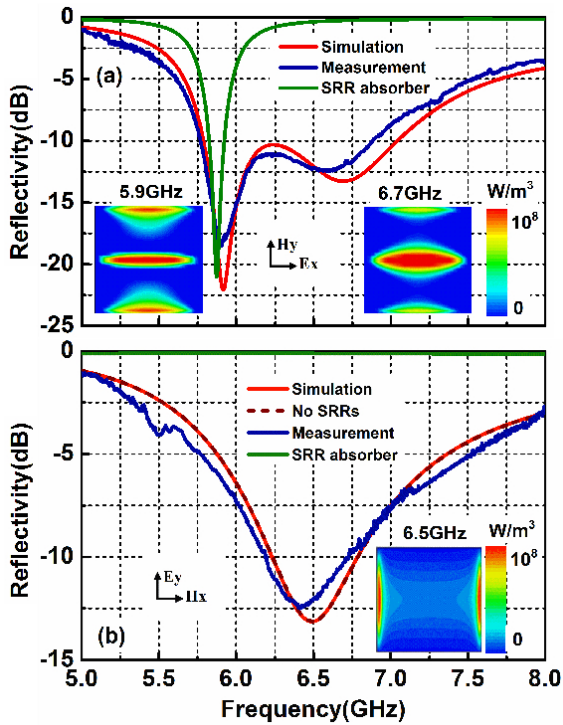
Fig. 14 - Simulated and measured reflectivity of the MM based absorber with the incident electric couple with SRR (a) and uncoupled (b). Dash line shows the reflectivity of the absorber without the SRR inclusions. Green curves show the simulated reflectivity of the SRR absorber. Inserts show the power loss density at the corresponding absorption peaks. (c) Photographs of the experimental prototypes: (a) SRRs and (b) the MM based absorber. Figure reproduced with permission [54]. Copyright 2012, Optical American Society.

It should be noted that the metal-backed SRR substrate also displays an absorption peak near 5.9 GHz proving that the absorption peak at 5.9 GHz is mainly related to the resonance of the metal-backed SRR substrate. When the incident electric field is perpendicular to the SRRs, neither an electrical response nor a magnetic response can be driven.

VIII. WIDEBAND ABSORBERS EMPLOYING RESONANT FSSs

The synthesis of wideband absorbers comprising a single FSS is achieved by inducing two resonances in the HIS cavity. From a circuital point of view, HIS cavity resonates for the second time when the inductive impedance of a suitably chosen FSS assumes the same absolute value with opposite sing of the capacitive impedance of the grounded substrate (thicker than a quarter wavelength). To this aim a resonant FSS element whose impedance changes from capacitive to inductive needs to be employed. The choice of a rather thick substrate guarantees also a sufficiently high value of the real part of Z_R in between the two parallel resonances. At the center of the operating band the absorption is still guaranteed since the substrate thickness equals $\lambda/4$ acting as an high-impedance wall ($Z=0+j\infty$) while the FSS impedance shows a purely real impedance (Salisbury screen condition). The optimal surface resistance can be derived from the equivalent circuit model assuming that the lumped resistance R of the equivalent circuit and the

surface resistance of the FSS R_S are approximately related as [20]:

$$R \approx R_s \frac{S}{A} \qquad (10)$$

where $S=D^2$, D is the cell periodicity and A is the surface area of the lossy element within a single unit cell. The relation implies that the smaller is the scattering area, the smaller is the surface resistance value leading to a fixed lumped resistance. It has to be pointed out that the optimal value of the surface resistance changes as a function of frequency [55]. When the substrate is air the following relation holds:

$$R_{opt}\left(\omega\right) = \frac{\varsigma_0}{2}\tan\left(k_0 d\right)\sin\left(2k_0 d\right) \qquad (11)$$

where ς_0 is the free space impedance d is the substrate thickness and k_0 is the propagation constant in free space. When the substrate thickness is equal to a quarter wavelength, the optimal value of lumped resistance becomes ς_0 (Salisbury screen case). It is convenient to choose an average value which guarantees a good matching over the entire bandwidth.

The working principle of the structure can be well understood by tracing the impedance curves on a Cartesian plot. Let us consider an FSS composed by a ring array with a periodicity D equal to 11 mm and a surface resistance R_s of 70 Ω/sq. The FSS layer is placed at 5 mm from the ground (the dielectric substrate is just air). The impedance of the grounded dielectric substrate and the impedance of the FSS, computed by retrieving full wave data of reflection coefficient, are reported in Fig. 15a. The two resonances previously mentioned and the Salisbury screen zone are highlighted in the figure. An optimal value of R_s to obtain a wide frequency range where the real part of Z_R is around 400 Ω which means 70 Ω/sq for a loop type patterned surface. In Fig. 15b the reflection coefficient of the absorber is also reported. The results obtained by using a periodic MoM code, Ansys HFSS and the equivalent circuit approach are compared and agree quite well.

The absorbing structure allows obtaining remarkable performance (-15 dB in the band from 7 GHz to 20 GHz) with an overall thickness of 5 mm only. Commercial Jaumann screens with similar performance are characterized by larger thickness. Despite the intrinsic periodicity of the structure, its dimension can be reduced down to a 4 by 4 array preserving almost the same absorption performances, with respect to a PEC plate of the same dimensions.

The use of double resonant FSS elements (fractal patch + cross [31] or double loops [56]) have been also investigated to improve the absorption bandwidth of the one-layer absorber. Their use can be useful to stabilize the FSS impedance behavior in correspondence of the center of the absorption bandwidth and thus creating a resonant peak within the so-called Salisbury zone.
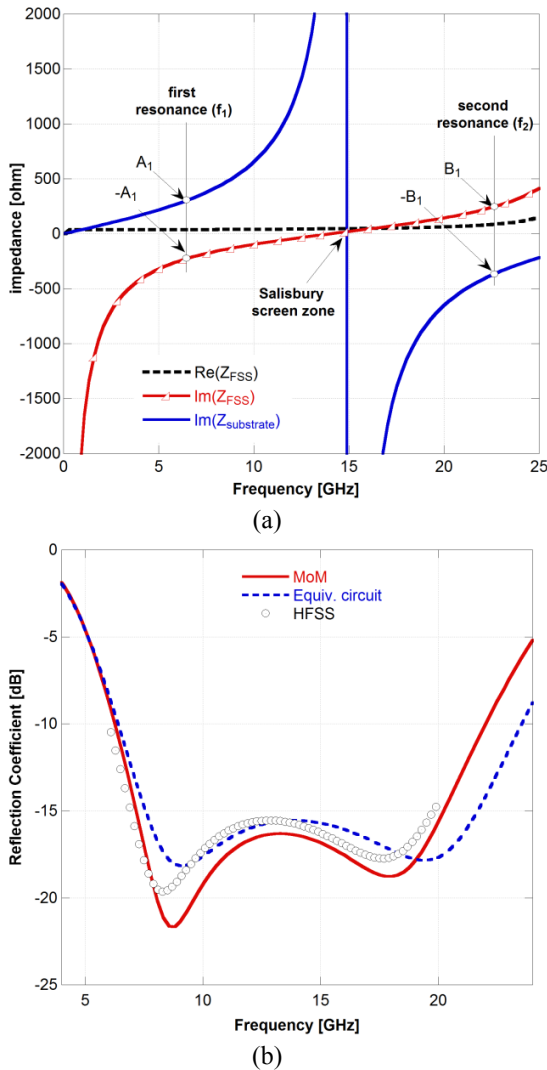
(a)

(b)

Fig. 15 – (a) Input impedance of a 5mm grounded air slab and impedance of a ring shaped FSS with periodicity D=11mm. The qualitative position of HIS resonances is highlighted. The real part in the FSS impedance will slightly shift those resonances (b) Reflection coefficient of the analyzed structure computed with MoM code, HFSS and equivalent circuit approach. Figure reproduced with permission [20]. Copyright 2010, IEEE.

The performance of the described absorbers based on resonant FSS structures is acceptable up to 30/40 degrees since they are not optimized for oblique incidence angles. A powerful method to improve the angular stability of the absorber consist in the employment of subwavelength capacitive elements in a multilayer configuration. This approach, which will be presented in the following sections, allows also avoiding the presence of grating lobes.

IX. Ultra-Wideband absorbers employing multilayer patch arrays

In microwave regime sometimes it is required to design an absorber capable of covering many frequency bands simultaneously. In such case, the bandwidth of the absorber may exceed 10:1 ratio (the ratio between the highest absorption frequency, F_h, to the lowest absorption frequency, F_l). Achieving such extremely large bandwidth

with few number of resistive FSS layers is a challenging problem. Resonating FSSs such as cross and loop elements, common in designing moderate bandwidth absorbers, are not suitable for this application. The first problem is to select the proper dimensions for the resonant elements. They must be sufficiently large to provide matching at the lowest frequency, while should be small enough to avoid grating lobes at the highest absorption frequency. Since the lowest and the highest absorption frequencies are largely separated from each other (10:1 ratio or more), it is very difficult to make a suitable tradeoff in the selection of the elements dimensions. Other problems related to resonant elements are the harmonics of the fundamental resonance and the anti-resonance frequencies which show their effects when the bandwidth becomes sufficiently large. Then, it is not possible to model the resonating FSS elements by a simple series LC circuit like the case of absorbers with moderate bandwidths. Moreover, one should control the anti-resonance frequencies in a way to avoid discontinuity in the absorption bandwidth. These mentioned problems force the designer to seek an alternative method for designing the ultra-wideband absorbers. Capacitive circuit method is such an alternative approach which can result in extremely large bandwidths in multi-layered configuration [33], [34]. In this approach, sub-wavelength low-pass arrays are used instead of the conventional resonating FSS elements. The low-pass arrays have capacitive impedance over the whole frequency band and, when they are made of resistive materials, they can be modeled by series RC circuits over the entire frequency band of interest. For this reason, this design approach is referred as *Capacitive Circuit Absorber* (CCA). Capacitive circuit absorber can provide extremely large bandwidth within a thicknesses close to optimal one.

The conventional method of designing large bandwidth frequency selective surface absorbers starts with defining a central frequency. Mostly such absorbers are designed by using low-permittivity spacers such as foam or honey-comb materials. The thicknesses of the dielectric layers are selected to be a quarter of wavelength at central frequency. In such way many degrees of freedom of the multilayer absorbing structure have been already removed. The remaining part of the design is to use the equivalent circuit model of the absorber to find suitable RLC circuits between the dielectric layers to provide matching over the frequency band of interest. Finally, the RLC circuits should be synthesized with proper resonating frequency selective surfaces, mainly loop shapes or cross dipoles.

When the absorption bandwidth is very broad with relative bandwidth ratios of 10:1 or larger, defining a central frequency becomes somehow meaningless. Therefore, one cannot follow the simple recipe of having quarter-wavelength distance between the FSS layers. Consequently, the proper selection of the thicknesses of dielectric layers will be an essential part of the design process. Usually the design objective is to achieve the desired bandwidth with minimum possible thickness. Capacitive circuit absorber method is a versatile method that is adopted in designs having different distances between the periodic layers. The design procedure begins with a circuit model of the absorber

which must be sufficiently accurate over the entire frequency band. This is easily accomplished by employing sub-wavelength non-resonating arrays. Low-pass periodic array of square patch elements with sub-wavelength spatial periodicity is one of the simplest forms chosen in the design of capacitive circuit absorbers. Such periodic arrays can be modeled very accurately by low-pass RC circuits over the entire frequency band of interest **[34], [57]**. In the following it is shown how the method can be employed to design an extremely wideband absorber with bandwidth ratio of 10.63 (F_h/F_l) while possessing a total thickness which is very close to the theoretical limit for the given frequency band **[33]**.

It is desired to design an extremely wideband absorber covering the frequency interval between 3 to 35 GHz, roughly. As mentioned the design procedure stats with an equivalent circuit model of the absorber. The top part of the Fig. 16 shows the equivalent circuit model of the capacitive circuit absorber. To cover such large bandwidth four layers of square patch arrays modeled by low-pass RC elements are required.
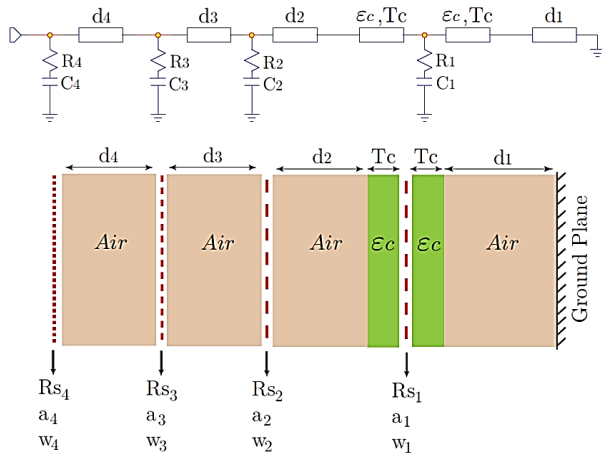

Fig. 16 - The schematic of the ultra-wideband absorber with optimal thickness. Top) The equivalent circuit model of the absorber. Bottom) The actual realization of the absorber. The resistive layers are periodic square patches with periodicity (a), width (w) and sheet resistivity (Rs). All the dielectric layers are considered to be air except the dielectric covers of the first resistive layer with parameters Tc = 0.2 mm and permittivity 4.4. Figure reproduced with permission [33]. Copyright 2011, IEEE.

The required values of the layer thicknesses and the RC values are obtained by the help of the equivalent circuit model, and they provide the largest practical bandwidth in the desired interval. The values of the circuit elements and the layer thicknesses are given in Table 1.

Table 1 - The parameters of the equivalent circuit model of the ultra-wideband capacitive circuit absorber.

Element index (n)	d_n [mm]	C_n (pF)	R_n (Ohm)
1	4.2	0.5	119.4
2	3.4	0.083	251.6
3	3.2	0.0316	505.8
4	3.3	0.024	886.8

Table 2 - The parameters of the equivalent circuit model of the ultra-wideband capacitive circuit absorber. Table reproduced with permission [33]. Copyright 2011, IEEE.

a_1 [mm]	a_2 [mm]	a_3 [mm]	a_4 [mm]
6.8	6.8	3.4	1.7
w_1 [mm]	w_2 [mm]	w_3 [mm]	w_4 [mm]
6.7	6.3	3	1.6
R_{s1} [Ohm/Sq]	R_{s2} [Ohm/Sq]	R_{s3} [Ohm/Sq]	R_{s4} [Ohm/Sq]
112.5	212	387.2	823.9

In contrast to conventional circuit analog absorbers with fixed layer thicknesses, the capacitive circuit absorber is capable of providing flexibility in selecting the dielectric layer thicknesses. It is of great importance when aiming for low profile designs with total thicknesses very close to theoretical limits (this topic will be addressed in the following sections) such as the current example. As seen from the Table 1, all the dielectric layers have different thicknesses with the largest value for the dielectric layer on top of the ground plane. When extremely large bandwidths are aimed for, the frequency selective surfaces used in the structure must provide matching at both very low and very high frequencies, simultaneously. Consequently, the reactive parts of their surface impedances possess significant differences in values among the different periodic layers, depending on the fact that they provide matching in different parts of the frequency band. That is the most challenging problem in using conventional resonating FSS elements for designing of UWB absorbers. Fortunately, it is possible and convenient to work with sub-wavelength low-pass elements for such designs. From Table 1 it is apparent that there is a considerably large contrast between the capacitance values of the first and the fourth layer ($C_1/C_4 \approx 20.8$). The is mainly due to the fact that the first layer is responsible for matching at low frequencies and the fourth layer helps to provide large bandwidth at high frequencies.

After calculating the different equivalent circuit parameters, the actual absorber must be synthesized by the help of proper periodic array of square patch elements. Since there is large difference among the required capacitance values of the layers, it is necessary to use different spatial periodicities among the periodic layers. In order to be able to simulate the electromagnetic properties of the synthesized design for verifying the performance of the obtained absorber, it is required that the periodic layers have commensurate periodicities. Otherwise, it will be extremely difficult to analyze the electromagnetic properties of the resulting aperiodic structure.

Table 2 provides the details of the unit cell element of the square patches used to synthesize the required RC values of the equivalent circuit model. In the table, a_i represents the periodicity, w_i the width of the square patches and Rsi the corresponding sheet resistivity of the i-th array (Fig. 16). The frequency response of the UWB absorber is shown in Fig. 17.
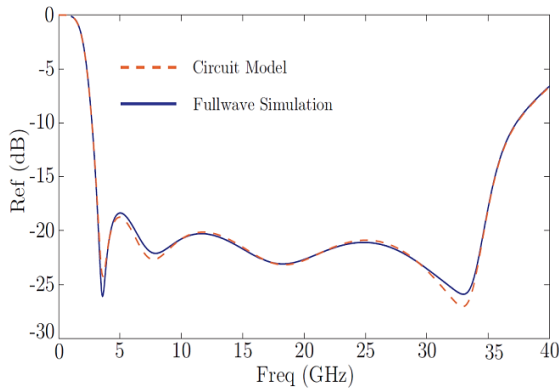
Fig. 17 - The frequency response of the ultra wideband absorber with optimal thickness obtained from both the equivalent circuit model and the full-wave simulation (CST Microwave Studio). The 20 dB absorption bandwidth covers the frequency interval 3.26_34.65 GHz, (fH/fL= 10.63). Figure reproduced with permission [33]. Copyright 2011, IEEE.

X. OPTIMAL DESIGN OF WIDEBAND ABSORBERS AT OBLIQUE INCIDENCE ANGLES

Frequency selective surfaces based absorbers are usually designed for normal angle of incidence using symmetrical shapes for the geometry of the unit cell. In this way the frequency response of the absorbers become polarization insensitive and the equivalent circuit models are simple enough to work with. In some applications it is required that the reflection from a surface is controlled at oblique angles of incidence e.g. RCS reduction from corners where multiple reflections can produce significant backscattering. At oblique angles of incidence the frequency response of FSS based absorbers becomes polarization dependent. Therefore, it is challenging to design an absorber that can operate over a wide scan angles for different impinging wave polarization. For example, the proposed via absorbers can only reduce the reflection for TM polarized wave. In this section, it is explained how the conventional design methods can be generalized and extended such that wideband scan angle independent polarization insensitive absorbers can be designed utilizing homogenous or periodic arrays of resistive sheets.

If the absorber is going to operate over a large angles of incidence for both principal polarizations (TE and TM), it is of great importance to work with frequency selective surfaces that can be modeled accurately for different incident angles and polarizations. For the resonating FSS types such as loops or cross dipoles, the resonant frequency, the bandwidth, the harmonic and anti-resonance frequencies of the periodic array, all vary with respect to angle of incidence and polarization. Consequently, it is very complicated to model them over a large bandwidth for different impinging wave angle and polarization. In contrast to resonating types, it has been shown that sub-wavelength sized arrays of square patches, used in capacitive circuit absorbers, can be modeled very accurately and simply by low-pass RC circuits over the entire frequency band of interest for a large range of scan angles at both TE/TM polarizations [32], [57]. As explained in [32] another important parameter in designing absorbers for oblique angle of incidence is to employ proper dielectric

layers in the design. The dielectric layers in the multilayered absorber are responsible for scan compensation, bandwidth increase and frequency response stabilizations. In the following, a capacitive circuit absorber able to provide an extremely large bandwidth of 26 GHz for oblique angles of incidence up to 45, degree for both TE and TM polarizations, is presented. The significance of the design can be emphasized by considering the fact that their rival design method using vias can only provide absorption for TM polarization and provide narrower bandwidths.

When the absorber is designed for oblique angles of incidence, the circuit models must be capable of modeling the effect of incidence angle and polarization. For dielectric layers it is very easy to generalize the equivalent model such that effect of polarization and scan angle are considered. A dielectric layer with physical thickness (d) and permittivity (ε) at incident angle (θ_i), is modeled by a transmission line with the equivalent electrical length (l) and intrinsic impedance/admittance (Z/Y) given as the following:

$$\cos(\theta) = \sqrt{(1 - \sin^2(\theta_i)/\varepsilon}$$

$$l = d\cos(\theta)$$

$$TE\ Polarization: Y = \sqrt{\varepsilon}\,Y_0\cos(\theta) \qquad (12)$$

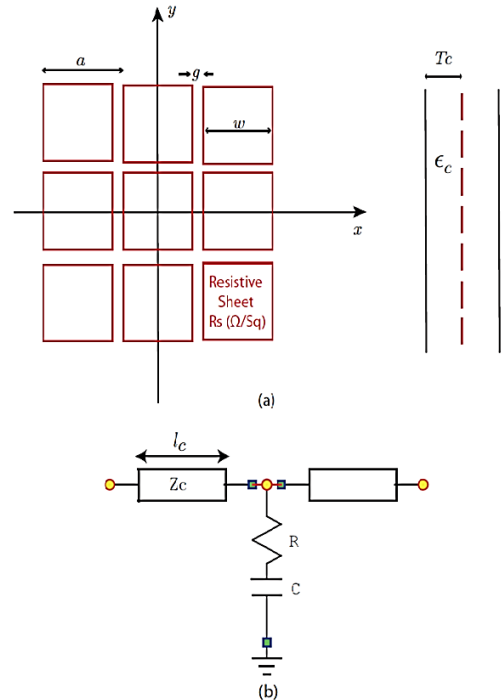$$TM\ Polarization: Z = \frac{Z_0}{\sqrt{\varepsilon}}\cos(\theta)$$

Fig. 18 - Periodic square patch array and its equivalent circuit model. (a) The front and the side view of the array embedded in dielectric (b) The equivalent circuit model of the periodic array and its parameters.

Modeling the frequency selective surface response can be a more complicated process. For resonating types if not impossible, it is a very detailed and complicated task to model all these effects by passive circuit elements. The

11

solution is to replace the resonating type elements with sub-wavelength size low-pass arrays such as periodic square patches. When the square patch array is embedded in a proper dielectric layer, the frequency response of the low-pass array can be modeled very accurately with simple RC elements over very broad bandwidths. Fig. 18 shows the geometry of a square patch array embedded in dielectric layer and its equivalent circuit model. The surrounding dielectric layer in which the low-pass array is embedded makes the values of the equivalent RC circuit approximately independent of incidence angle and polarization. An example is provided in Table 3 that lists the computed values of the equivalent RC values for a typical square patch element at different incident angles at both TE and TM polarizations.

Table 3 - The resistance (R) and the capacitance (C) values of the circuit model for a typical square patch array at different angles of incidence and polarizations. (ϵ=2.3 ,Tc = 0.2 mm, a= 4.3 mm, w=4.1 mm, Rs = 100 Ohm/Sq).

Θ (deg)	TE		TM	
	R[Ohm]	C [pF]	R[Ohm]	C [pF]
0	114	0.121	114	0.121
15	114	0.125	113.5	0.125
30	116	0.121	114	0.121
45	118	0.127	114	0.126
60	119.5	0.129	114	0.126

The behavior can be easily understood if the analytic expression of the patch array capacitance obtained through the averaged approach is considered. While the capacitance of patch array is independent of incident angle for TM polarization **[57]**, the capacitance has an angular variation for TE polarization:**[57], [58]**:

$$C_{patch}^{TE} \simeq \frac{D\varepsilon_0 \left(\varepsilon_{eff}\right)}{2\pi} \ln\left(\frac{1}{\sin\left(\frac{\pi w}{2D}\right)}\right)\left(1 - \frac{\sin^2\left(\vartheta_i\right)}{2\sqrt{\varepsilon_{eff}}}\right) \quad (13)$$

where $keff = k_0\sqrt{\varepsilon_{eff}}$ is the wave number of the incident wave vector in the effective host medium, $\varepsilon_{eff} = \left(\varepsilon_{up} + \varepsilon_{down}\right)/2$ represents the effective permittivity of an equivalent uniform medium composed by the two dielectrics surrounding the grid, D is the grid period, w is the strip width and μ_0, k_0 are, respectively, the permeability and the wave number in free space. It is evident that increasing the effective permittivity of the surrounding medium tends to reduce angular dependence of the array.

Now that all elements of the multilayered absorber are accurately described by equivalent circuit models, the next step will be to adopt such models to design an ultra-wide band capacitive circuit absorber for oblique angles of incidence. For this purpose, the incidence angles in the interval [0-45] degree are considered. In this way, three different circuit models must be considered simultaneously:

1. The equivalent circuit model of absorber for normal angle of incidence.
2. The equivalent circuit model at 45 degree angle of incidence and TE polarization.
3. The equivalent circuit model at 45 degree angle of incidence and TM polarization.

Because the square patches used to synthesize the RC elements of the equivalent circuits have geometrical symmetry, the frequency response is polarization insensitive at normal angle of incidence. Therefore, only one circuit model is sufficient to model normal incidence illumination. Although three circuit models are required to model the frequency response of the absorber, it is important to note that these models are not independent from each other. The design process is a multi-objective problem which should match three dependent circuit models simultaneously. An example is provided in the following Fig. 19 where the schematic of a multilayered capacitive circuit absorber designed by the above mentioned circuit models is shown.
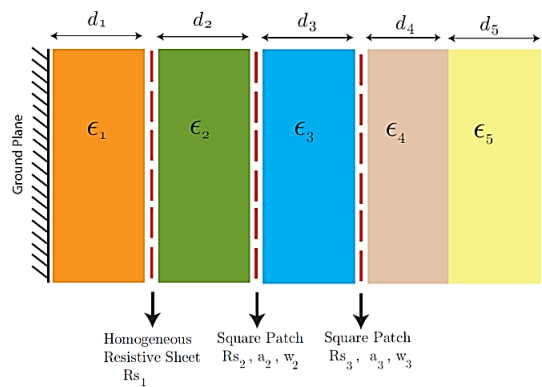

Fig. 19 - The schematic of the multilayered capacitive circuit absorber for oblique angle of incidence.

The first resistive sheet employed in the design is a homogenous layer while the rest are made of resistive square patches. All the resistive sheets are embedded in a similar dielectric layer with T_c=0.2 mm and ε=2.3, see Fig. 18. The parameters of the dielectric layers are listed in Table 4 and the dimension of the square patches and their corresponding sheet resistivity are given in Table 5. These patches are used to synthesize the RC elements of the equivalent circuit models with the values tabulated in Table 6. The full-wave simulation of the absorber frequency response is shown in Fig. 20. The design provides an extremely large absorption bandwidth at both normal and oblique angles of incidence. More importantly, both TE and TM polarizations are absorbed by the structure, in contrast to the designs using via concept working only at TM polarization. Sensitivity analysis shows that the proposed design is very robust and small changes in parameters do not affect the absorption response [32]. This is another important feature of the capacitive circuit absorber method.

Table 4 - The parameters of the dielectric layers used in the capacitive circuit design.

d_1 [mm]	d_2 [mm]	d_3[mm]	d_4 [mm]	d_5 [mm]
3.4	2.6	2.4	3.3	4
ϵ_1	ϵ_2	ϵ_3	ϵ_4	ϵ_5
1.8	1.7	1.33	1.8	1.33

Table 5 - The dimensions of the square patch arrays (a) periodicity, (w) width. The fundamental spatial period of the absorber is 3.6 mm.

a_2 [mm]	w_2 [mm]	a_3 [mm]	w_3 [mm]
3.6	3.5	1.8	1.6

Table 6 - The values of the series RC elements used in the circuit model of the capacitive absorber.

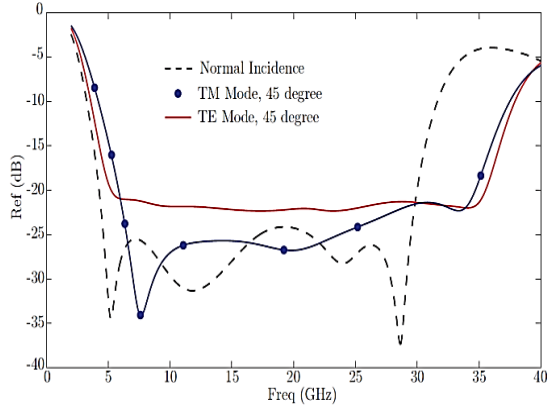| R_1 [Ohm]	R_2 [Ohm]	R_3 [Ohm]
134	308.5	486.5
C_1 (pF)	C_2 (pF)	C_3 (pF)
---	0.136	0.039

Fig. 20 - The frequency response of the capacitive circuit absorber at normal and oblique angle of incidence. Figure reproduced with permission [32]. Copyright 2010, IEEE.

XI. TUNABLE ABSORBERS

Several mechanisms have been investigated to make the absorber response adaptable. Some of the main mechanisms will be briefly introduced in this section:

- Diode loaded FSSs;
- Liquid crystal substrates;
- Conductivity change of the periodic patterns

- *a) Lumped loaded FSSs*

By loading the frequency selective surfaces with varactor diodes or MEMS (Micro Electro-Mechanical Systems) on each unit cell, the distributed capacitance of the periodic surface can be dynamically controlled. If we represent the impedance of the capacitive patch array as a lumped capacitor ($Z_{patch}^{TE/TM} = 1/j\omega C_{patch}$), the connection of an active device can be represented with a lumped element impedance in parallel to the FSS impedance. The simplified equivalent circuit of the active capacitive FSS is shown in Fig. 21. The varactor diode is modelled as a series of a resistor R_{var} and a capacitor C_{var}. Assuming that the value of the resistor is small enough (below 10 Ω) we can assume that the total capacitance of the FSS is:

$$C_{loaded\_FSS} \approx C_{var} + C_{patch}$$

On the other hand, the new series resistance which represents losses has the following expression:

$$R_{loaded\_FSS} \approx \frac{R_{var}C_{var}^2}{\left(C_{var} + C_{patch}\right)^2} \qquad (14)$$

If the capacitance of the varactor is of the same order of magnitude of the patch array capacitance, the effect of the diode resistor is equivalent to·R_{var}/4. At this stage, the losses of the high-impedance ground plane can be studied as ones of a HIS composed by a resistive FSS [20].
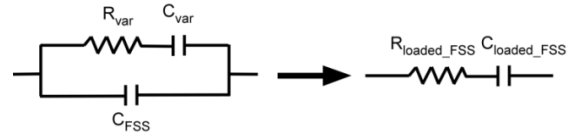

Fig. 21 - Modelization of the patch array loaded with varactor diodes.

As an example, we examine the reflection behavior of an FSS comprising a 6.525 mm × 5.925 mm patch, repeated with a periodicity of 8.9 mm. The dimension of the resonator fits with those of a WR137 waveguide so that only a few diode are necessary to experimentally verify the dynamic behavior of the surface. The reflection coefficient of the structure, simulated by Ansoft HFSS, are reported in Fig. 22.

The main drawback related with varactor-loaded absorber is the use of a huge number of active devices necessary to implement a panel of some wavelengths. For instance, a relatively small panel comprising 30 unit cells along the planar directions requires a 1800 varactors. If we consider the unit price of microwave varactors (several euros each), it is therefore easy to expect an unpractical final cost of a reconfigurable HIS panel. The conventional loading of a single varactor for each of the unit cells of the frequency selective surface can be overcome by connecting the FSS unit cells to a feeding network located behind the ground plane through metalized vias. At the center of the feeding network a single varactor is applied to tune a high-impedance surface composed for instance by 8 unit cells [59]. The tuning capability of the single-diode structure is reduced with respect to the configuration with eight diodes because of the dispersive characteristics of the modified varactor network but the re-configurability potentiality could be sufficient for some applications.

Such tunable AMC absorbing ground planes can be also adopted to improve the low-frequency absorption properties of a commercial Salisbury screen [22], [60]. Indeed, the use of the tunable AMC ground plane in place of the electric ground allows to add a tunable absorption band at low-frequency without significant modification of the thickness of the structure and its in-band absorption properties.
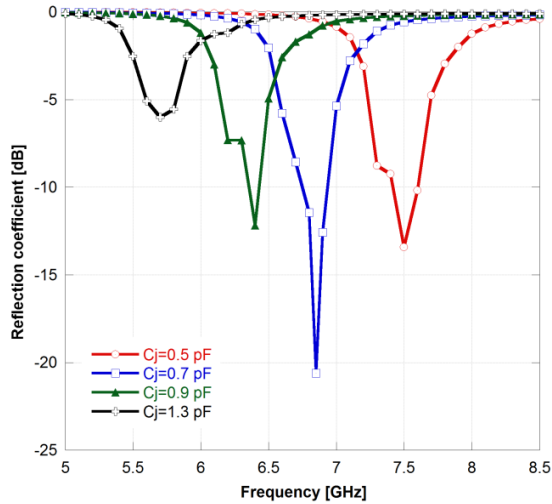
Fig. 22 - Reflection coefficient of a varactor loaded absorber comprising a patch FSS on a thin (0.8 mm) FR4 grounded substrate.
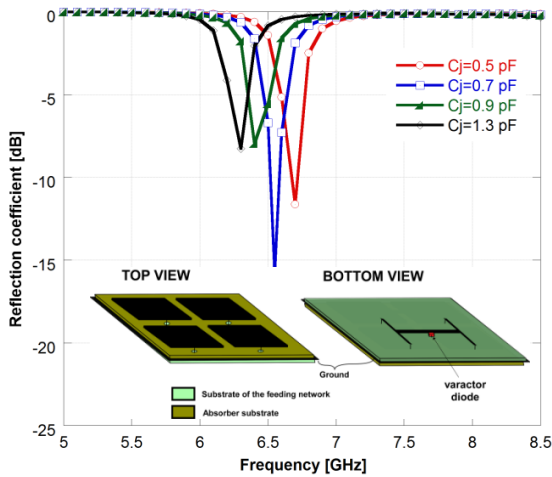

Fig. 23 - Reflection coefficient of a varactor loaded absorber obtained by printing FSS patches on a thin (0.8 mm) FR4 grounded substrate.

- *b) Liquid crystal substrates*

Liquid Crystal (LC) substrates may be used to dynamically control the resonant behavior of the absorber. Indeed, dielectric permittivity of the LC substrates can be varied by applying a DC, or a low frequency AC, bias voltage, that is, a torque necessary to rotate molecules from perpendicular (permittivity $\varepsilon_\perp$) to parallel orientation (permittivity $\varepsilon_{//}$). As a result, the permittivity of the tunable substrate varies between two values (biased state) and (0 V state) and therefore the dielectric anisotropy is given by

$$\Delta\varepsilon = \varepsilon_{//} - \varepsilon_\perp.$$

The properties of some LC mixtures measured in the literature across different frequency range are summarized Table 7. LC were initially employed to design tunable reflectarrays whose layout is geometrically similar to that of recently proposed tunable metamaterial absorbers. The difference is that the reflectarray aims to obtain a low loss reflection coefficient whereas the absorber is designed to

minimize the reflection coefficient amplitude. By using one of the substrates reported in Table 7, an example of LC tunable absorber can be designed. For simplicity, only the liquid crystal mixture is considered as substrate even if in practice the LC must be confined in a closed structure formed by other thin dielectrics. Since the permittivity variation between biased and unbiased states is quite limited the tunability of LC absorbers is much lower than that obtained with varactor loaded structures.

- *c) Conductivity change of periodic patterns*

The variation of the surface resistance of the periodic patterns can be also used to modulate or tune the absorbing properties of the resonant HIS absorbers.
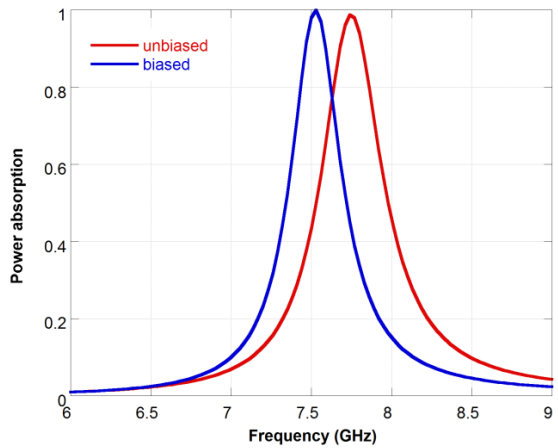

Fig. 24 - Power absorption of a LC absorber based on a Jerusalem cross FSS printed on top of a grounded MERCK K15 LC substrate. The biased and unbiased curves are obtained by using the parameters listed in table 1.

Table 7 – Properties of two liquid crystal mixtures obtained within two different frequency range.

Type of LC	Frequency [GHz]	$\varepsilon_{//}$ (biased)	$\varepsilon_\perp$ (0V)
MERCK K15 LC	5	2.9-j0.087	2.7-j0.108
LC MDA 03-2838	35	3.1-j0.0124	2.3-j0.0253
MERCK BL037 LC	110-170	3.2-j0.064	2.8-j0.056
LC 5CB	2600	4	3.3

There exist some materials that are able to change their conductivity when a DC voltage is applied to them. Two popular materials are Indium Thin oxide (ITO) and Graphene. ITO is a heavily-doped n-type semiconductor with a large bandgap which makes it mostly transparent in the visible part of the spectrum [61]. Graphene is a zero-gap semiconductor formed by pure carbon in the form of a very thin (one atom thick) nearly transparent sheet [62]. ITO is used in a large variety of applications (e.g. liquid crystal displays, touch panels, solar cells) since it can be precisely etched into fine patterns [63] but it has some drawbacks including high cost due to limited supply of indium, costly layer deposition, fragility and lack of flexibility [64], [65]. Graphene allows dynamic control of both real and imaginary part of the conductivity when a DC voltage is applied. In microwave range graphene can guarantee a change of the real part of graphene conductivity while in THz range also

14

the imaginary part of the graphene conductivity can be changed since plasma frequency of graphene is in THz range, which is much lower than noble metals.

A change of the real part of conductivity can guarantee a absorption modulation while a dynamic control of the imaginary part can be efficiently used to achieve a tunable device. The main limitation of graphene is that the process of separating it from graphite requires technological development to be economical enough for industrial processes. This is the reason why today, graphene is not used in commercial applications.

Graphene can be modeled by surface conductivity tensor which depends on several parameters as well as electrical and magnetic field bias [66]. Since graphene behaves as resistive material at microwave frequencies, it can be efficiently employed to time modulate the reflection properties of a FSS absorbers [67]. In Fig. 25 the reflection properties of the single layer wideband absorber as a function of the surface resistance of the loops is reported. Realistic values of both surface resistance and modulation factor (5 to 7) [68] of graphene have been employed. A large reflectivity modulation is attainable which can be eventually employed to dynamically change the radar cross section of target and antennas [5] with a relatively simple setup.
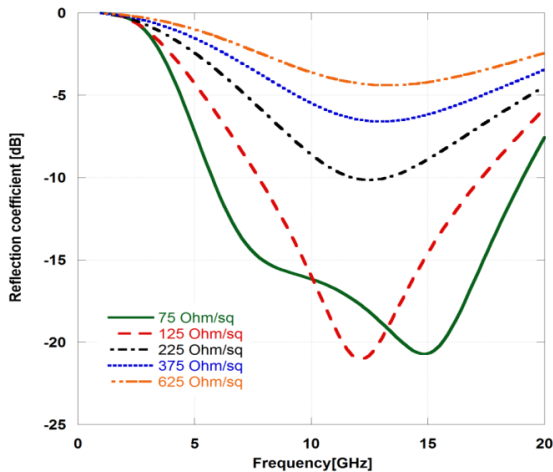

Fig. 25 – Absorption properties modulation obtained by changing the surface resistance of periodic loops in wideband single layer absorber presented in section V.
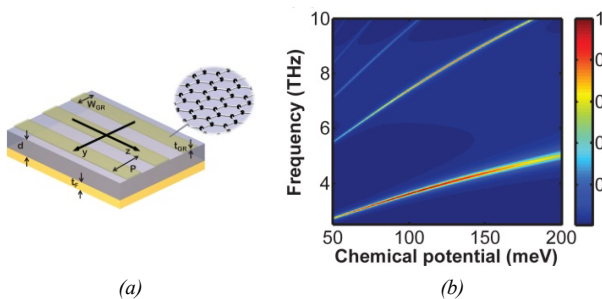

(a)   *(b)*

Fig. 26 – (a) Schematic of the graphene micro-ribbon perfect absorber. (b) Absorption as a function of frequency and chemical potential for graphene micro-ribbons perfect absorber with d = 4.7 μm at normal incidence. Figure reproduced with permission [69]. Copyright 2012, The Optical Society.

As already pointed out, in THz range graphene is characterized by the plasmonic behavior which allows to dynamically control also the imaginary part of the surface resistance. This interesting property can be exploited to design a tunable absorber [69]. The layout of the absorber and its performance as a function of the chemical potential as shown in Fig. 26.

XII. PHYSICAL LIMITATIONS

Recently, many publications have dealt with absorbers. The designs include metamaterial, electromagnetic bandgap, high impedance surfaces, or more traditional approaches such as frequency selective surfaces. Mostly, in all approaches the aim is to provide the largest possible bandwidth for a given absorber thickness. It is observed that the bandwidth of the absorber is somehow related to its total thickness. With single layer absorbers only moderate bandwidths can be achieved and for wideband applications multilayered designs are necessary. This experimental observation leads to a theoretical question. Is there a physical relation between the absorption bandwidth and the total thickness of an absorber? In order to answer this question it is important to note that all the above mentioned approaches, used for designing absorbers, have one common feature among them. They are all composed of periodic arrangement of passive, linear, time invariant, and casual materials. Rozanov has shown that for any metal-backed absorber the infinite integral of the reflectance is bounded from above under certain conditions [70]. The conditions are very general and include all linear, passive, time invariant and causal materials. Under these conditions the complex permittivity and permeability of the materials obey the Kramers-Kronig relations. If the exp(jωt) time dependence is considered for the incident wave, then the reflection coefficient is analytic in the lower half-plane of complex angular frequency (ω) [70]. Thus, it can be shown that the following physical bound exists:

$$\left| \int_0^\infty ln|R(\lambda)| d\lambda \right| \le 2\pi^2 \sum_i \mu_{s,i} d_i \qquad (15)$$

In the above equation R is the reflection coefficient, λ is the wavelength in free space and d_i, μ_i are the thickness and the static permeability of the layer i of the multilayer slab. For nonmagnetic absorbers, the above equation can be rearranged into the following form:

$$d \ge \frac{\left| \int_0^\infty ln|R(\lambda)| d\lambda \right|}{2\pi^2} \qquad (16)$$

The above equation states that for a given absorption frequency response, the total thickness of the absorber d cannot be less than a theoretical limit. This minimum possible thickness can be used as an evaluation tool to judge the efficiency of a design method.

Some of the above analyzed configurations are compared against the minimum theoretical thickness according to (16). The results are summarized in Table 8. It is evident that such designs are very close to the theoretical limit.

Table 8 - Electrical and geometrical parameters of the analyzed wideband and ultra-wideband absorbing structures. The physical limit is computed according to (16).

Number of layers	Thickness [mm]	Electrical thickness	Physical limit [mm]	Pattern period [mm]	FSS element
1	5	$0.12\lambda_{max}$	4.5	11	loop
3	15.1	$0.17\lambda_{max}$	13.3	10	patch
4	14.5	$0.135\lambda_{max}$	13.8	6.8	patch

XIII. PRACTICAL MANUFACTURING OF ABSORBERS

FSS-based absorbers characterized by ultra-narrowband response are manufactured by using a standard photolithographic etching process of commercial substrates such as FR4. Indeed, dielectric losses of commercial substrate are sufficient to obtain a total absorption of incident electromagnetic fields if all the parameters of the resonators are opportunely set. The higher are the losses of the substrate, the higher is the substrate thickness that is necessary to guarantee a perfect matching with free space impedance. Realization of metamaterial absorbers in the THz domain requires sub-micron lithography [71]. An example of such THZ narrowband absorbers is shown in Fig. 27.

Metamaterial absorbers are usually investigated within THz gap but they can be potentially employed in microwave region for applications where narrow frequency bands are used, e.g. UHF-RFID systems (865 MHz – 868 MHz) [25], [72]. Conventional $\lambda/4$ absorbers would be too thick in UHF band (around 8.5 cm) and magnetically loaded absorber are too heavy. As an example a metamaterial absorber based on a commercial FR4 substrate can be designed to operate around 868 MHz. with a thickness of 3.2 mm, that is, lower than $\lambda_0/100$ at the operating frequency. Since the use of standard photolithographic process on commercial FR4 substrates at sub-GHz frequencies leads to heavy and expensive metamaterial absorbers, conventional cardboard panels have been proposed as a substrate and conductive spray paint or with a shaped aluminum foil to realized metallic patterns [25]. Prototypes of metamaterial absorbers operating across UHF band are reported in Fig. 28.
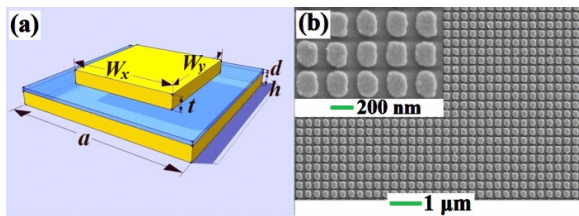

Fig. 27 - (a) Laout of the patch metamaterial absorber operating in the infrared frequency band. Wx and Wy represent, respectively, the side lengths of rectangular metallic particle along the x and y axis and t represents its thickness. d and h , respectively, denote the thicknesses of the Al2O3 dielectric layer and the gold film. a is the lattice constant. (b) Top view SEM image of the fabricated optical metamaterial absorber. Figure reproduced with permission **[71]**. Copyright 2012, American Institute of Physics
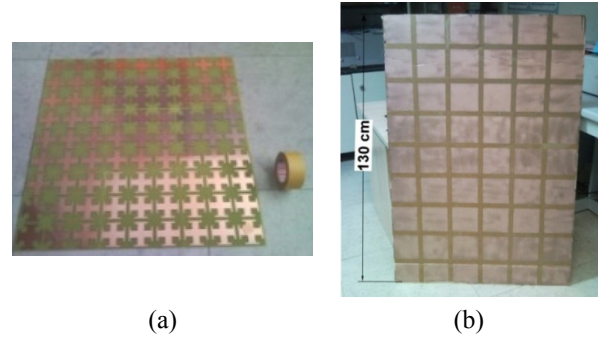

(a)   (b)

Fig. 28 - (a) Prototype of a metamaterial absorber operating across UHF frequency band. The FSS unit cell is formed by a Jerusalem cross and the substrate is a 3.2 mm FR4 slab. The back side of FR4 is uniformly metalized. Figure reproduced with permission [73]. Copyright 2013, IEICE. (b) A picture of a patch array FSS manufactured with a conductive spray deposition on top of a 6.5 mm thick cardboard grounded substrate. Figure reproduced with permission [25]. Copyright 2014, IEEE.

Practical realization of resistive FSSs with controlled surface resistance values necessary for synthesizing wideband and ultra-wideband absorbers are extensively reported in literature over the last few years. The most popular realization technique is silk printing process. Physical vapor deposition (PVD) can be also used for reducing the tolerances on the value of the surface resistance but at an increased realization cost.

(a)   (b)

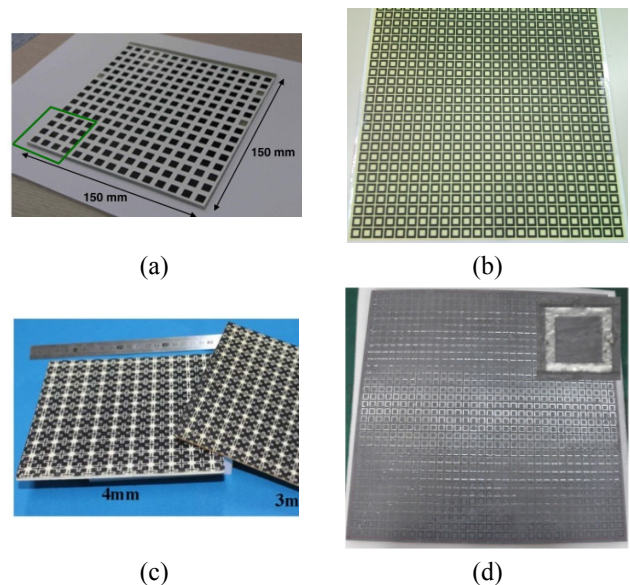(c)   (d)

Fig. 29 – A prototype of an FSS based absorber obtained by applying a conductive polymer through screen printing. (a) Figure reproduced with permission [59]. Copyright 2008, Elsevier. (b) Figure reproduced with permission [20]. Copyright 2010, IEEE. (c) Figure reproduced with permission **[31]**. Copyright 2012, Optical American Society. (d) Figure reproduced with permission **[75]**. Copyright 2013, Institute of Physics (IOP).

One of the first prototypes of resistive FSS [74] is shown in Fig. 29a. Other prototypes with more complicated FSS elements obtained through screen printing are reported in Fig. 29b and Fig. 29c. Another method to manufacture resistive surfaces has been recently proposed in [75] resistive plastic sheets are patterned through laser cutting. This latter

specimen is reported in Fig. 29d. Resistive loaded FSS can be also obtained by using lumped resistors. Some manufactured samples operating in microwave range [18], [76] are reported in Fig. 30. It has to be pointed out that the practical manufacturing of large boards requires a huge number of microwave lumped resistors which are not low-cost. The realization of resistive loaded FSS through resistive paints has also additional advantages with respect lumped loaded metallic FSS, that is, the weight and the flexibility of the board.
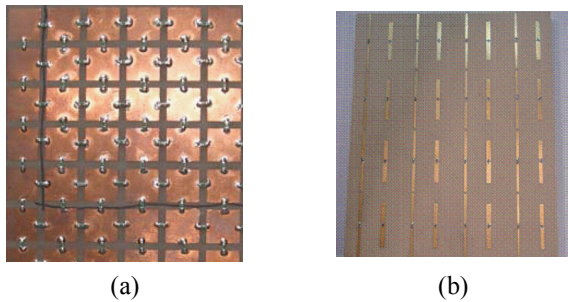

(a)   (b)

Fig. 30 – (a) Narrowband absorber comprising lumped loaded patches. Figure reproduced with permission [18]. Copyright 2006, EuMA. (b) Wideband absorber comprising lumped loaded dipoles. Figure reproduced with permission [76]. Copyright 2007, IEEE.

XIV.   PROMISING APPLICATIONS OF FSS-ABSORBERS

FSS-based absorbers have proved to be a versatile structure that has been exploited in a very wide range of applications.

One of the most investigated area is related to stealth technology and more precisely to the reduction of the Radar Cross Section (RCS) of antennas. Resistive periodic surfaces have been adopted for reducing the field scattered by a 2x2 patch array [1] by surrounding the antennas with the absorber. An absorbing selective radome has been designed in [2] for allowing the in-band radiation of the enclosed antenna and, at the same time, the reduction of the scattered field in the out-of-band. FSS-based absorbers have been tailored to enhance the stealth performance of a patch array antenna comprising a hybrid ground plane [3]. In this case, the insertion of an absorber placed below the selective transparent ground plane (Fig. 31) has doubled the low-RCS bandwidth of the antenna. In [5] a superstrate comprising a resistive periodic surface and parasitic metallic patches has been presented as a good trade-off for reducing the RCS of a slot array and improving the radiation properties of the antenna.

Another application of FSS-based absorbers that is lately gaining interest is related the control of the signal propagation within an indoor environment. In particular, ultrathin absorbing panels [25], [72] have been proposed for reducing multiple reflection interference in UHF RFID systems operating in warehouses or offices. The use of absorbers can prevent false, incorrect or multiple readings caused by undesired propagation paths. FSS-based absorbers allow the implementation of structures with reduced thickness, if compared to a Salisbury screen, and minimum weight if compared with solution exploiting ferrite materials.

Signal propagation may be controlled also for security reasons as described in [77] where a dual-layer absorb/transmit surface is designed for absorbing WLAN signals while passing mobile ones.
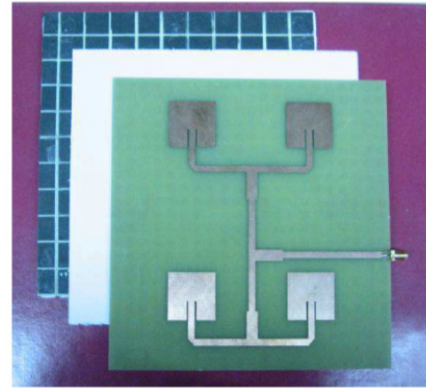

Fig. 31 – Prototype of the antenna with the selective transparent ground plane enhanced by a suitable-designed FSS-absorber. Figure reproduced with permission. Courtesy of The Electromagnetics Academy [3].

In the framework of radio identification, multi-resonant absorbers have been recently proposed as RFID chipless tags in [47] where a compact tag comprising few unit cells of the FSS-based absorber can be designed to exhibit perfect absorption at same predefined frequencies. This multi-band absorber can store bits of information by allowing a "total reflection" state and a "total absorption" state at each predefined frequency to encode '0' and '1', respectively. Some examples of the manufactured low-profile chipless RFID tags are reported in Fig. 32.

Fig. 32 – Prototypes of chipless RFID tags of different dimensions (2x2 and 3x3 unit cells). Figure reproduced with permission [47]. Copyright 2013, IEEE.

A very promising application of FSS-based absorbers is their employment in Thermophotovoltaic (TPV) systems. In TPV system the heat is converted into electricity by radiating thermal-generated photons able to generate electron-hole pairs in a low-bandgap photovoltaic medium and thus a current. In solar TPV systems the sunlight is collected via optical concentrators and it is then absorbed by a surface which is coupled with an emitter that radiates photons which impinges on a photovoltaic (PV) cell. More in detail, photons with energy less than the bandgap of the PV converter cannot

be absorbed to generate electron/hole pairs and are either reflected and lost or passes through the cell. Photons with energy above the bandgap can be absorbed, but the excess energy is lost, thus generating undesirable heating in the cell and reducing the efficiency. In a TPV system it is advantageous to match the thermal emission with the most efficient conversion characteristics of the photovoltaic cell therefore it is of the utmost importance to control the emitter properties. In this scenario, a selective emitter whose thermal radiation is much narrower than that of a blackbody at the same temperature would improve the system performance. FSS-based absorbers can play this role because they can be tailored to have sharp resonances with high absorption and thus, thanks to the Kirchhoff's law of thermal radiation, they can realize a high-Q emitter with high emissivity [78][79]. Absorbers can be customized for exhibiting a desired emissivity even over a large bandwidth as in [11] where a FSS-based absorber is engineered with multiple different-size unit cell to reproduce the external quantum efficiency (EQE) of gallium antimonide (GaSb) in a wavelength dependent fashion.
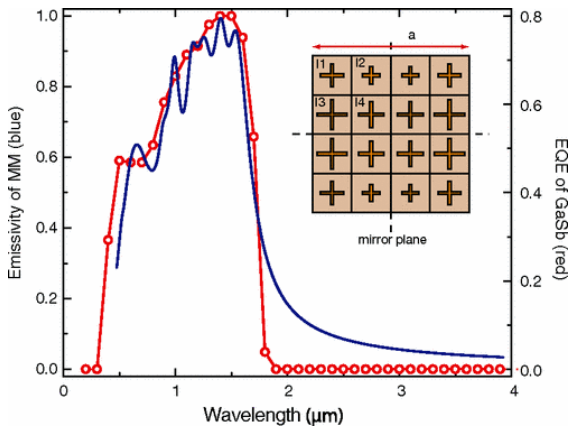

Fig. 33 – Examples of FSS-based absorbers in TPV system design. Designed metamaterial emissivity (blue curve) and EQE (red curve) of GaSb. Inset shows a schematic of the metamaterial design with 16 sublattices. Dimensions of the design are a ¼ 1080 nm, l1 ¼ 173 nm, l2 ¼ 127 nm, l3 ¼ 221:5 nm, l4 ¼ 190 nm. Each cross sublattice has a line width of 20 nm and thickness of 50 nm. The thickness of the dielectric spacer is 78.8 nm and the ground plane is 200 nm. The unit cell also possesses two mirror planes, one horizontal and one vertical, as noted. Figure reproduced with permission [11]. Copyright 2011, American Physical Society.

Absorbers are also receiving an increasing attention as fundamental building blocks of sensors and imaging systems. In fact, designing a compact absorbing surface can improve the capability of EM detectors, especially in the THZ frequency regime. A Terahertz detector based on an engineered FSS-based absorber has been proposed in [80]. More in detail, each pixel of the detector comprises a THz wave absorber, a cantilever with a large coefficient of thermal expansion and a reflective surface. At the pixel resonance, the THz radiation is absorbed and produces heat. This heat determines the mechanical deflection of the cantilever which is sensed by the optical deflection operated by the reflective surface (Fig. 34). A plasmonic sensor operating in the Near-Infrared (NIR) regime is described in

[81] by combining the concepts of perfect absorption with the localized surface plasmon resonance.
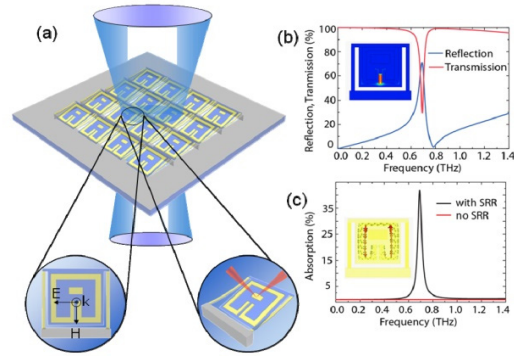

Fig. 34 – Metamaterial enhanced terahertz detector using optical readout. (a). Schematic of the device showing the metamaterial cantilever array, an individual pixel, and reflective optical read-out. (b). Numerical simulation of the transmission reflection and transmission of the device. (Inset) Simulated electric field distribution on resonance (693GHz). (c). Numerical simulation of the absorption of the device with (black line) and without (red line) split ring resonators (SRRs). (Inset) Simulated surface current on resonance. Figure reproduced with permission [80]. Copyright 2011, The Optical Society.

Another THz imaging system is described in [82] where a multispectral sensor (0.3, 0.33 and 0.36 THz) is realized with polarization-sensitive absorbing pixel. When the absorption of a pixel takes place and induces a sufficient pixel heating, an underneath graphitized layer serves as infrared emissive layer which is subsequently detected by an IR camera (Fig. 35).
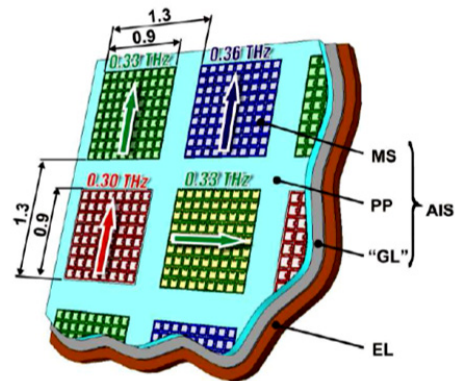

Fig. 35 – Scheme of matrix structure of the absorbers: metasurface (MS), polypropylene film (PP), metal ground layer (GL), IR emissive layer (EL). Arrows indicate the direction of the linear polarization corresponding to the maximal absorption. Figure reproduced with permission. Courtesy of The Electromagnetics Academy [82].

Absorbers have been also proposed as detectors of microwave radiation. In [83] an FSS-based absorber unit cell converts the incident microwave radiation into an electric current which is then driven to a receiver chain which is able to infer the power associated to the impinging signal (Fig. 36). A similar concept is adopted in [7] to capture a 2D image of the RF power distribution and in [84] for measuring the 2D distribution of a RF filed both in amplitude and phase.
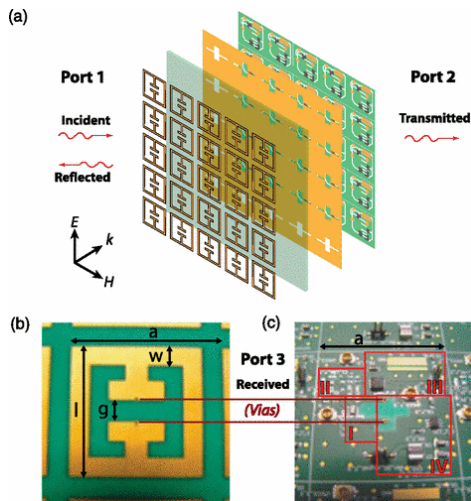
Fig. 36 – System architecture of metamaterial microwave power detector array. (a) Radiation is incident from port 1 with electric field polarization as depicted. (b) Photo of an individual pixel (c) Photo of the circuit layer with vias indicated. The vias transport the received signal (port 3) to the microwave power receiver circuit underneath each unit cell where the different highlighted regions are: (I) balun, (II) impedance matching circuit, (III) low noise amplifier, and IV) microwavepower detector. Figure reproduced with permission [83]. Copyright 2012, American Physical Society.

XV. OPEN ISSUES AND FUTURE DIRECTIONS

In the last decade the topic of electromagnetic absorbers has seen a renewed interest fostered by the growing number of applications. The focus of this paper was on thin electromagnetic absorbers synthesized by employing periodic surfaces and artificial impedance surfaces since this type of configuration has showed very interesting properties both in terms of manufacturing simplicity and in terms of versatility of the achievable performance. It has been shown that the HIS based absorbers are able providing absorption bandwidth spanning from few percent to decade always keeping the thickness of the structure very close to physical limitations. The design of the absorber can be efficiently carried out by exploiting equivalent circuit models which provide a reliable platform to studying physical phenomena involved in the absorption phenomenon as well as to optimize the unit cell design of the periodic surface once the bandwidth requirements and substrate properties have been fixed. A considerable number of papers dealing with new types of absorbing configurations based on HIS still appear in the literature but is our opinion that the use of a unit cell instead of another does not add relevant information. The main directions for research on this topic are probably the comprehension of the physical phenomena involved in the different absorbing mechanisms through new detailed but still simple models as well as the proposal of new applications of both narrow-band or wideband absorbers design. Some promising applications still need a deeper investigation. For example, in the THz range, imaging applications seem a promising topic for narrow-band absorbers. In microwave regime, the properties of absorbers on three-dimensional objects and their ability to reduce the scattering cross-section of complex objects has not been fully addressed. Another aspect, which is still under study, is the

manufacturing of lossy periodic surfaces. Some fabrication processes have been reported for the manufacturing of periodic surfaces with a controlled surface resistance, however there is still not a standard procedure. It has been remarked that the use of lossy materials, e.g. graphite based inks or non-perfect conductors, is preferable with respect to the integrations of lumped components on a periodic metallic surface. Finally, an interesting field of research is represented by the tunability of absorbers, with mechanisms simple enough to have chance to be employed in practice. Indeed, even if some tunable structures have been demonstrated in the literature by using active components (liquid crystal or graphene), they still remain a good exercise because of the very high manufacturing costs of panel having large areas.

XVI. CONCLUSIONS

Properties of the electrically thin absorbers synthesized by employing opportunely designed high-impedance surfaces are discussed. The differences between an entirely metallic absorber, typically referred to as metamaterial absorber, and HIS absorbers comprising resistive FSSs are highlighted by recurring to a simple transmission line model. It is shown that dielectric losses are predominant for metamaterial absorbers while ohmic losses are the most influent in case of resistive losses. Techniques to improve the operating bandwidth or to design multi-resonant absorbers have been described. Properties and performance of single-layer and multi-layer absorbers have been also introduced. Manufacturing procedures of the described absorbing structures have been also presented. Finally, promising applications and open issues have been described.

REFERENCES

[1] H.-K. Jang, J.-H. Shin, and C.-G. Kim, "Low RCS patch array antenna with electromagnetic bandgap using a conducting polymer," in *International Conference on Electromagnetics in Advanced Applications (ICEAA), 2010*, 2010, pp. 140–143.

[2] F. Costa and A. Monorchio, "A frequency selective radome with wideband absorbing properties," *IEEE Trans. Antennas Propag.*, vol. 60, no. 6, pp. 2740–2747, 2012.

[3] F. Costa, S. Genovesi, and A. Monorchio, "A frequency selective absorbing ground plane for low-RCS microstrip antenna arrays," *Prog. Electromagn. Res.*, vol. 126, pp. 317–332, 2012.

[4] S. Genovesi, F. Costa, and A. Monorchio, "Low-profile array with reduced radar cross section by using hybrid frequency selective surfaces," *IEEE Trans. Antennas Propag.*, vol. 60, no. 5, pp. 2327–2335, 2012.

[5] S. Genovesi, F. Costa, and A. Monorchio, "Wideband Radar Cross Section Reduction of Slot Antennas Arrays," *IEEE Trans. Antennas Propag.*, vol. 62, no. 1, pp. 163–173, Jan. 2014.

[6] D. Weston, *Electromagnetic Compatibility: Principles and Applications, Revised and Expanded*. CRC Press, 2001.

[7] S. Yagitani, K. Katsuda, M. Nojima, Y. Yoshimura, and H. Sugiura, "Imaging radio-frequency power distributions by an EBG absorber," *IEICE Trans. Commun.*, vol. 94, no. 8, pp. 2306–2315, 2011.

[8] T. Maier and H. Brückl, "Wavelength-tunable microbolometers with metamaterial absorbers," *Opt. Lett.*, vol. 34, no. 19, pp. 3012–3014, 2009.

[9] S. A. Kuznetsov, A. G. Paulish, A. V. Gelfand, P. A. Lazorskiy, and V. N. Fedorinin, "Bolometric THz-to-IR converter for terahertz imaging," *Appl. Phys. Lett.*, vol. 99, no. 2, p. 023501, 2011.

[10] H.-T. Chen, W. J. Padilla, M. J. Cich, A. K. Azad, R. D. Averitt, and A. J. Taylor, "A metamaterial solid-state terahertz phase modulator," *Nat. Photonics*, vol. 3, no. 3, pp. 148–151, 2009.

[11] X. Liu, T. Tyler, T. Starr, A. F. Starr, N. M. Jokerst, and W. J. Padilla, "Taming the blackbody with infrared metamaterials as selective thermal emitters," *Phys. Rev. Lett.*, vol. 107, no. 4, p. 045901, 2011.

[12] J.-J. Greffet, "Applied physics: Controlled incandescence," *Nature*, vol. 478, no. 7368, pp. 191–192, 2011.

[13] E. F. Knott, J. Shaeffer, and M. Tuley, *Radar Cross Section, Second Edition*. SciTech Publishing, 2004.

[14] B. Chambers, "Frequency tuning characteristics of capacitively loaded Salisbury screen radar absorber," *Electron. Lett.*, vol. 30, no. 19, pp. 1626–1628, Sep. 1994.

[15] E. F. Knott and C. D. Lunden, "The two-sheet capacitive Jaumann absorber," *IEEE Trans. Antennas Propag.*, vol. 43, no. 11, pp. 1339–1343, Nov. 1995.

[16] B. A. Munk, *Frequency Selective Surfaces: Theory and Design*. John Wiley & Sons, 2005.

[17] B. A. Munk, P. Munk, and J. Pryor, "On designing Jaumann and circuit analog absorbers (CA absorbers) for oblique angle of incidence," *IEEE Trans. Antennas Propag.*, vol. 55, no. 1, pp. 186–193, 2007.

[18] S. W. Simms and V. F. Fusco, "Thin Radar Absorber Using an Artificial Magnetic Ground Plane," in *Microwave Conference, 2006. 36th European*, 2006, pp. 1167–1169.

[19] H. Mosallaei and K. Sarabandi, "A one-layer ultra-thin meta-surface absorber," in *2005 IEEE Antennas and Propagation Society International Symposium*, 2005, vol. 1B, pp. 615–618 vol. 1B.

[20] F. Costa, A. Monorchio, and G. Manara, "Analysis and design of ultra thin electromagnetic absorbers comprising resistively loaded high impedance surfaces," *IEEE Trans. Antennas Propag.*, vol. 58, no. 5, pp. 1551–1558, 2010.

[21] F. Terracher and G. Berginc, "Thin electromagnetic absorber using frequency selective surfaces," in *IEEE Antennas and Propagation Society International Symposium, 2000*, 2000, vol. 2, pp. 846–849 vol.2.

[22] F. Costa and A. Monorchio, "Multiband electromagnetic wave absorber based on reactive impedance ground planes," *Microw. Antennas Propag. IET*, vol. 4, no. 11, pp. 1720–1727, 2010.

[23] F. Che Seman, R. Cahill, V. F. Fusco, and G. Goussetis, "Design of a Salisbury screen absorber using frequency selective surfaces to improve bandwidth and angular stability performance," *IET Microw. Antennas Propag.*, vol. 5, no. 2, p. 149, 2011.

[24] N. I. Landy, S. Sajuyigbe, J. J. Mock, D. R. Smith, and W. J. Padilla, "Perfect metamaterial absorber," *Phys. Rev. Lett.*, vol. 100, no. 20, p. 207402, 2008.

[25] F. Costa, S. Genovesi, A. Monorchio, and G. Manara, "Low-Cost Metamaterial Absorbers for Sub-GHz Wireless Systems," *IEEE Antennas Wirel. Propag. Lett.*, vol. 13, pp. 27–30, 2014.

[26] G. Manara, A. Monorchio, and R. Mittra, "Frequency selective surface design based on genetic algorithm," *Electron. Lett.*, vol. 35, no. 17, pp. 1400–1401, 1999.

[27] D. J. Kern and D. H. Werner, "A genetic algorithm approach to the design of ultra-thin electromagnetic bandgap absorbers," *Microw. Opt. Technol. Lett.*, vol. 38, no. 1, pp. 61–64, Jul. 2003.

[28] Y. Tsuda, T. Yasuzumi, and O. Hashimoto, "A Thin Wave Absorber Using Closely Placed Divided Conductive Film and Resistive Film," *Antennas Wirel. Propag. Lett. IEEE*, vol. 10, pp. 892–895, 2011.

[29] Y.-Q. Li, H. Zhang, Y.-Q. Fu, and N.-C. Yuan, "RCS reduction of ridged waveguide slot antenna array using EBG radar absorbing material," *Antennas Wirel. Propag. Lett. IEEE*, vol. 7, pp. 473–476, 2008.

[30] D. Sjöberg, "Analysis of wave propagation in stratified structures using circuit analogues, with application to electromagnetic absorbers," *Eur. J. Phys.*, vol. 29, no. 4, p. 721, 2008.

[31] L. Sun, H. Cheng, Y. Zhou, and J. Wang, "Broadband metamaterial absorber based on coupling resistive frequency selective surface," *Opt. Express*, vol. 20, no. 4, pp. 4675–4680, 2012.

[32] A. Kazemzadeh and A. Karlsson, "Multilayered wideband absorbers for oblique angle of incidence," *IEEE Trans. Antennas Propag.*, vol. 58, no. 11, pp. 3637–3646, 2010.

[33] A. Kazemzadeh, "Nonmagnetic ultrawideband absorber with optimal thickness," *IEEE Trans. Antennas Propag.*, vol. 59, no. 1, pp. 135–140, 2011.

[34] A. K. Zadeh and A. Karlsson, "Capacitive circuit method for fast and efficient design of wideband radar absorbers," *IEEE Trans. Antennas Propag.*, vol. 57, no. 8, pp. 2307–2314, 2009.

[35] F. Costa, S. Genovesi, A. Monorchio, and G. Manara, "A circuit-based model for the interpretation of perfect metamaterial absorbers," *IEEE Trans. Antennas Propag.*, vol. 61, no. 3, pp. 1201–1209, 2013.

[36] F. Costa and A. Monorchio, "Closed-form analysis of reflection losses in microstrip reflectarray antennas," *IEEE Trans. Antennas Propag.*, vol. 60, no. 10, pp. 4650–4660, 2012.

[37] J. E. Raynolds, B. A. Munk, J. B. Pryor, and R. J. Marhefka, "Ohmic loss in frequency-selective surfaces," *J. Appl. Phys.*, vol. 93, no. 9, pp. 5346–5358, 2003.

[38] F. Costa and A. Monorchio, "Electromagnetic Absorbers based on High-Impedance Surfaces: From ultra-narrowband to ultra-wideband absorption," *Adv. Electromagn.*, vol. 1, no. 3, pp. 7–12, 2012.

[39] R. Mittra, C. H. Chan, and T. Cwik, "Techniques for analyzing frequency selective surfaces-a review," *Proc. IEEE*, vol. 76, no. 12, pp. 1593–1615, Dec. 1988.

[40] F. Costa, S. Genovesi, and A. Monorchio, "On the bandwidth of high-impedance frequency selective surfaces," *Antennas Wirel. Propag. Lett. IEEE*, vol. 8, pp. 1341–1344, 2009.

[41] R. Diaz, "Magnetic loading of artificial magnetic conductors for bandwidth enhancement," in *IEEE Antennas and Propagation Society International Symposium, 2003*, 2003, vol. 2, pp. 431–434 vol.2.

[42] D. J. Kern and D. H. Werner, "Magnetic loading of EBG AMC ground planes and ultrathin absorbers for improved bandwidth performance and reduced size," *Microw. Opt. Technol. Lett.*, vol. 48, no. 12, pp. 2468–2471, Dec. 2006.

[43] L. Sun, H. Cheng, Y. Zhou, and J. Wang, "Design of a Lightweight Magnetic Radar Absorber Embedded With Resistive FSS," *IEEE Antennas Wirel. Propag. Lett.*, vol. 11, pp. 675–677, 2012.

[44] H. Wakatsuchi, S. Greedy, C. Christopoulos, and J. Paul, "Customised broadband metamaterial absorbers for arbitrary polarisation," *Opt. Express*, vol. 18, no. 21, pp. 22187–22198, 2010.

[45] H. Yang, X. Cao, J. Gao, W. Li, Z. Yuan, and K. Shang, "Low RCS metamaterial absorber and extending bandwidth based on electromagnetic resonances," *Prog. Electromagn. Res. M*, vol. 33, pp. 31–44, 2013.

[46] F. Costa, A. Monorchio, and G. Manara, "Efficient analysis of frequency-selective surfaces by a simple equivalent-circuit model," *Antennas Propag. Mag. IEEE*, vol. 54, no. 4, pp. 35–48, 2012.

[47] F. Costa, S. Genovesi, and A. Monorchio, "A Chipless RFID Based on Multiresonant High-Impedance Surfaces," *Microw. Theory Tech. IEEE Trans. On*, vol. 61, no. 1, pp. 146–153, 2013.

[48] J. Brown, "Artificial dielectrics having refractive indices less than unity," *Proc. IEE - Part IV Inst. Monogr.*, vol. 100, no. 5, pp. 51–62, Oct. 1953.

[49] W. Rotman, "Plasma simulation by artificial dielectrics and parallel-plate media," *IRE Trans. Antennas Propag.*, vol. 10, no. 1, pp. 82–95, Jan. 1962.

[50] P. A. Belov, R. Marques, S. I. Maslovski, I. S. Nefedov, M. Silveirinha, C. R. Simovski, and S. A. Tretyakov, "Strong spatial dispersion in wire media in the very large wavelength limit," *Phys. Rev. B*, vol. 67, no. 11, p. 113103, 2003.

[51] O. Luukkonen, P. Alitalo, F. Costa, C. Simovski, A. Monorchio, and S. Tretyakov, "Experimental verification of the suppression of spatial dispersion in artificial plasma," *Appl. Phys. Lett.*, vol. 96, no. 8, p. 081501, 2010.

[52] O. Luukkonen, F. Costa, C. R. Simovski, A. Monorchio, and S. A. Tretyakov, "A thin electromagnetic absorber for wide incidence angles and both polarizations," *IEEE Trans. Antennas Propag.*, vol. 57, no. 10, pp. 3119–3125, 2009.

[53] O. Luukkonen, M. G. Silveirinha, A. B. Yakovlev, C. R. Simovski, I. S. Nefedov, and S. A. Tretyakov, "Effects of Spatial Dispersion on Reflection From Mushroom-Type Artificial Impedance Surfaces," *IEEE Trans. Microw. Theory Tech.*, vol. 57, no. 11, pp. 2692–2699, Nov. 2009.

[54] Y. Pang, H. Cheng, Y. Zhou, Z. Li, and J. Wang, "Ultrathin and broadband high impedance surface absorbers based on metamaterial substrates," *Opt. Express*, vol. 20, no. 11, pp. 12515–12520, 2012.

[55] H.-B. Zhang, P.-H. Zhou, H.-P. Lu, Y.-Q. Xu, D.-F. Liang, and L.-J. Deng, "Resistance selection of high impedance surface absorbers for perfect and broadband absorption," *IEEE Trans. Antennas Propag.*, vol. 61, no. 2, pp. 976–979, 2013.

[56] Y. Shang, Z. Shen, and S. Xiao, "On the Design of Single-Layer Circuit Analog Absorber Using Double-Square-Loop Array," *IEEE Trans. Antennas Propag.*, vol. 61, no. 12, pp. 6022–6029, Dec. 2013.

[57] O. Luukkonen, C. Simovski, G. Granet, G. Goussetis, D. Lioubtchenko, A. V. Raisanen, and S. A. Tretyakov, "Simple and accurate analytical model of planar grids and high-impedance surfaces comprising metal strips or patches," *IEEE Trans. Antennas Propag.*, vol. 56, no. 6, pp. 1624–1632, 2008.

[58] F. Costa and A. Monorchio, "Design of subwavelength tunable and steerable Fabry-Perot/leaky wave antennas," *Prog. Electromagn. Res.*, vol. 111, pp. 467–481, 2011.

[59] F. Costa, A. Monorchio, and G. P. Vastante, "Tunable high-impedance surface with a reduced number of varactors," *Antennas Wirel. Propag. Lett. IEEE*, vol. 10, pp. 11–13, 2011.

[60] F. C. Seman, R. Cahill, and V. F. Fusco, "Salisbury screen with reduced angular sensitivity," *Electron. Lett.*, vol. 45, no. 3, pp. 147–149, Jan. 2009.

[61] H. Kim, C. M. Gilmore, A. Pique, J. S. Horwitz, H. Mattoussi, H. Murata, Z. H. Kafafi, and D. B. Chrisey, "Electrical, optical, and structural properties of indium–tin–oxide thin films for organic light-emitting devices," *J. Appl. Phys.*, vol. 86, no. 11, pp. 6451–6461, 1999.

[62] A. K. Geim and K. S. Novoselov, "The rise of graphene," *Nat. Mater.*, vol. 6, no. 3, pp. 183–191, 2007.

[63] D. S. Ginley, H. Hosono, and D. C. Paine, "Handbook of transparent conductors," 2010.

[64] F. Yi, E. Shim, A. Y. Zhu, H. Zhu, J. C. Reed, and E. Cubukcu, "Voltage tuning of plasmonic absorbers by indium tin oxide," *Appl. Phys. Lett.*, vol. 102, no. 22, p. 221102, 2013.

[65] A. Melikyan, N. Lindenmann, S. Walheim, P. M. Leufke, S. Ulrich, J. Ye, P. Vincze, H. Hahn, T. Schimmel, and C. Koos, "Surface plasmon polariton absorption modulator," *Opt. Express*, vol. 19, no. 9, pp. 8855–8869, 2011.

[66] J. Perruisseau-Carrier, "Graphene for antenna applications: Opportunities and challenges from microwaves to THz," in *Antennas and Propagation*

Conference (LAPC), 2012 Loughborough, 2012, pp. 1–4.

[67] A. Fallahi and J. Perruisseau-Carrier, "Design of tunable biperiodic graphene metasurfaces," *Phys. Rev. B*, vol. 86, no. 19, p. 195408, 2012.

[68] S. Bae, H. Kim, Y. Lee, X. Xu, J.-S. Park, Y. Zheng, J. Balakrishnan, T. Lei, H. R. Kim, and Y. I. Song, "Roll-to-roll production of 30-inch graphene films for transparent electrodes," *Nat. Nanotechnol.*, vol. 5, no. 8, pp. 574–578, 2010.

[69] R. Alaee, M. Farhat, C. Rockstuhl, and F. Lederer, "A perfect absorber made of a graphene micro-ribbon metamaterial," *Opt. Express*, vol. 20, no. 27, p. 28017, Dec. 2012.

[70] K. N. Rozanov, "Ultimate thickness to bandwidth ratio of radar absorbers," *IEEE Trans. Antennas Propag.*, vol. 48, no. 8, pp. 1230–1234, 2000.

[71] J. Hao, J. Wang, X. Liu, W. J. Padilla, L. Zhou, and M. Qiu, "High performance optical absorber based on a plasmonic metamaterial," *Appl. Phys. Lett.*, vol. 96, no. 25, p. 251104, 2010.

[72] Y. Okano, S. Ogino, and K. Ishikawa, "Development of Optically Transparent Ultrathin Microwave Absorber for Ultrahigh-Frequency RF Identification System," *IEEE Trans. Microw. Theory Tech.*, vol. 60, no. 8, pp. 2456–2464, Aug. 2012.

[73] F. Costa, S. Genovesi, A. Monorchio, and G. Manara, "Perfect metamaterial absorbers in the ultra-high frequency range," in *Electromagnetic Theory (EMTS), Proceedings of 2013 URSI International Symposium on*, 2013, pp. 701–703.

[74] W.-J. Lee, J.-W. Lee, and C.-G. Kim, "Characteristics of an electromagnetic wave absorbing composite structure with a conducting polymer electromagnetic bandgap (EBG) in the X-band," *Compos. Sci. Technol.*, vol. 68, no. 12, pp. 2485–2489, Sep. 2008.

[75] L. Liu and H. Cha, "Analysis and design of the invisible radome by LLumar glass," *J. Phys. Appl. Phys.*, vol. 47, no. 7, p. 075105, 2014.

[76] Z. Shen, B. Zheng, Z. Mei, J. Yang, and W. Tang, "On the design of wide-band and thin absorbers using the multiple resonances concept," in *International Conference on Microwave and Millimeter Wave Technology, 2008. ICMMT 2008*, 2008, vol. 1, pp. 32–35.

[77] G. I. Kiani, A. R. Weily, and K. P. Esselle, "A novel absorb/transmit FSS for secure indoor wireless networks with reduced multipath fading," *IEEE Microw. Wirel. Compon. Lett.*, vol. 16, no. 6, pp. 378–380, Jun. 2006.

[78] C. Wu, B. Neuner III, J. John, A. Milder, B. Zollars, S. Savoy, and G. Shvets, "Metamaterial-based integrated plasmonic absorber/emitter for solar thermo-photovoltaic systems," *J. Opt.*, vol. 14, no. 2, p. 024005, Feb. 2012.

[79] S. Thongrattanasiri, F. H. L. Koppens, and F. J. García de Abajo, "Complete Optical Absorption in Periodically Patterned Graphene," *Phys. Rev. Lett.*, vol. 108, no. 4, Jan. 2012.

[80] H. Tao, E. A. Kadlec, A. C. Strikwerda, K. Fan, W. J. Padilla, R. D. Averitt, E. A. Shaner, and X. Zhang, "Microwave and terahertz wave sensing with metamaterials," *Opt. Express*, vol. 19, no. 22, pp. 21620–21626, 2011.

[81] N. Liu, M. Mesch, T. Weiss, M. Hentschel, and H. Giessen, "Infrared Perfect Absorber and Its Application As Plasmonic Sensor," *Nano Lett.*, vol. 10, no. 7, pp. 2342–2348, Jul. 2010.

[82] S. A. Kuznetsov, A. G. Paulish, A. V. Gelfand, P. A. Lazorskiy, and V. N. Fedorinin, "Matrix structure of metamaterial absorbers for multispectral terahertz imaging," *Prog. Electromagn. Res.*, vol. 122, pp. 93–103, 2012.

[83] D. Shrekenhamer, W. Xu, S. Venkatesh, D. Schurig, S. Sonkusale, and W. J. Padilla, "Experimental Realization of a Metamaterial Detector Focal Plane Array," *Phys. Rev. Lett.*, vol. 109, no. 17, Oct. 2012.

[84] S. Yagitani, T. Sunahara, T. Nakagawa, D. Hiraki, Y. Yoshimura, and H. Sugiura, "Radio-frequency field measurement using thin artificial magnetic conductor absorber," in *Electromagnetic Theory (EMTS), Proceedings of 2013 URSI International Symposium on*, 2013, pp. 691–694.

Photo

Bio